The intracellular bacterium *Orientia tsutsugamushi* hijacks the adaptor protein BICD2 for dynein-based motility

Giulia Manigrasso[1], Kittirat Saharat[2], Chitrasak Kullapanich[3], Jerome Buolanger[1], Tomos E. Morgan[1], Holger Kramer[1†], Jeanne Salje[2,3,4,5*] and Andrew P. Carter[1*]

1. MRC Laboratory of Molecular Biology, Cambridge, CB2 0QH, UK
2. Cambridge Institute for Medical Research, University of Cambridge, CB2 0XY, Cambridge, UK
3. Mahidol-Oxford Tropical Medicine Research Unit, Faculty of Tropical Medicine, Mahidol University, Bangkok, 10400, Thailand
4. Department of Pathology, University of Cambridge, Cambridge, CB2 1QP, UK
5. Department of Biochemistry, University of Cambridge, Cambridge, CB2 1GA, UK

† Deceased

* Correspondence to cartera@mrc-lmb.cam.ac.uk and jss53@cam.ac.uk

ABSTRACT

The intracellular bacterium *Orientia tsutsugamushi* relies on the microtubule cytoskeleton and the motor protein dynein to traffic to the perinuclear region within infected cells. However, it remains unclear how the bacterium is coupled to the dynein machinery and how transport is regulated. Here, we discover that *O. tsutsugamushi* uses its autotransporter protein ScaC to recruit the dynein adaptor BICD2 to the bacterial surface. We show that ScaC is sufficient to engage dynein-based motility in the absence of other bacterial proteins and that BICD2 is required for efficient movement of *O. tsutsugamushi* during infection. Using TIRF single-molecule assays, we demonstrate that ScaC induces BICD2 to adopt an open conformation which activates the assembly of dynein-dynactin complexes. Our results reveal a novel role for BICD2 during bacterial infection and provide mechanistic insights into the life cycle of an important human pathogen.

INTRODUCTION

Many intracellular bacteria hijack the host cytoskeleton to acquire motility for their infection cycle. Whereas the most common strategy involves manipulation of actin assembly[1], a small group of bacteria, including *Chlamydia trachomatis* and *Orientia tsutsugamushi*, have developed the ability to exploit microtubules[2-4]. Both *C. trachomatis* and *O. tsutsugamushi* move along microtubule tracks to reach their subcellular niche[2,4]. However, while *Chlamydia* remains encased within endocytic membranes, thus leveraging the host vesicular transport system, *O. tsutsugamushi* resides free in the cytosol and needs to establish direct connections with microtubule motors. Therefore, *O. tsutsugamushi* is a fascinating model to study the interplay between intracellular pathogens and the microtubule cytoskeleton.

Orientia tsutsugamushi is an obligate intracellular bacterium which is transmitted to mammalian hosts through the bite of mite larvae[5,6]. Infection in humans causes the potentially life-threatening disease scrub typhus, whose symptoms include fever, skin rash, myalgia and, in severe cases, multiple organ failure[6-8]. *O. tsutsugamushi* colonizes a range of host cell types, including endothelial cells and leukocytes of the innate immune system[9,10]. Entry into host cells occurs via clathrin-mediated endocytosis and macrophagocytosis and is followed by rapid disruption of the phagosomal membrane to release the bacteria into the cytosol[11,12]. Cytosolic *O. tsutsugamushi* are transported along microtubules to the perinuclear region, where bacterial replication takes place[2]. Exit from infected host cells involves a budding-like mechanism, akin to the exit strategy employed by enveloped viruses, which releases membrane-enclosed bacteria into the extracellular space[13,14].

Transport of *O. tsutsugamushi* to the perinucleus requires the motor protein dynein and its essential cofactor dynactin[2]. Together, these two macromolecules form a complex which powers the long-range retrograde transport of cellular cargoes[15]. Efficient movement requires a coiled-coil component known as an activating adaptor,

which facilitates the interaction between dynein and dynactin while recruiting the transport machinery to its cargo[16,17]. More than 15 activating adaptors have been described so far, each connecting the motile complex to a specific cargo[15,18]. Although the role of dynein in *O. tsutsugamushi* movement is known, it remains unclear which bacterial effectors are required for transport. Furthermore, it is unknown whether the association between *O. tsutsugamushi* and dynein is direct or mediated by host factors such as activating adaptors.

Here, we show that *O. tsutsugamushi* uses the autotransporter protein ScaC, which sits on the bacterial outer membrane[19-21], to recruit the activating adaptors BICD1 and BICD2 to its surface. Ectopically expressed ScaC engages dynein in the absence of other bacterial proteins, suggesting it is sufficient for the initiation of motility. We use size exclusion chromatography and single-molecule motility assays to demonstrate that ScaC promotes an open conformation of BICD2, which in turn facilitates the interaction with dynein and dynactin. Finally, we show that BICD2 is required for efficient perinuclear migration of *O. tsutsugamushi*. Overall, our study uncovers a novel pathway for bacterial motility along microtubules.

RESULTS

The bacterial protein ScaC recruits the activating adaptors BICD1 and BICD2

Since *O. tsutsugamushi* is not surrounded by host membranes, we reasoned that it must have developed ways to directly recruit dynein to its surface. Bacterial proteins that sit on the outer membrane are likely candidates for this process as they are easily accessible to host factors in the cytosol. Among these, members of the surface cell antigen (Sca) family of autotransporters are especially interesting as they possess a large extracellular domain capable of interacting with the host cell machinery and have been implicated in actin-based motility in *Rickettsia* species[22,23]. Sca proteins comprise a conserved C-terminal translocator domain and a variable N-terminal passenger domain. The translocator domain forms a pore in the bacterial outer membrane which in turn enables the translocation of the passenger domain to the cell surface. To determine whether Sca proteins are involved in the interaction with dynein, we expressed the passenger domains of four Sca family members conserved across diverse *O. tsutsugamushi* strains (ScaA, ScaC, ScaD and ScaE) fused to a N-terminal GFP tag in Flp-In HeLa cells, and performed pull-downs followed by protein identification by mass spectrometry (Fig.1A). None of the hits for ScaA, ScaD and ScaE had known links to dynein (Supplementary Fig. 1A, Supplementary Tables 1-3). On the other hand, the passenger domain of ScaC (residues 33-223, hereafter referred to as ScaC) co-precipitated BICD1 and BICD2, which are paralogs and both members of the Bicaudal D (BICD) family of activating adaptors (Fig. 1B, Supplementary Table 4)[16,17,24].

To confirm that ScaC can engage the dynein machinery to drive motility, we performed a mitochondrial relocation assay in HeLa cells. In this approach, a protein of interest is targeted to the mitochondrial outer membrane using a membrane targeting sequence (MTS) and the subcellular localization of the organelles is monitored by fluorescence microscopy (Fig. 1C)[25,26]. An accumulation of mitochondria at the perinuclear region provides evidence that the candidate protein is a dynein effector [25,27,28]. We generated Flp-in T-REX HeLa cell lines expressing GFP^{MTS} or GFP-ScaC^{MTS} fusion proteins. As a positive control, we used a GFP-BICD2N^{MTS} line expressing the constitutively active N-terminal fragment of BICD2 (residues 1-400, BICD2N), which is known to elicit dynein-based motility and has been used extensively in organelle relocation assays (Supplementary Fig. 1B)[25,26,28]. GFP^{MTS} expression did not alter the distribution of mitochondria, which remained scattered in the cytoplasm as observed in wild type cells (Fig. 1D-E, Supplementary Fig. 1C-D). Conversely, GFP-ScaC^{MTS} caused dramatic perinuclear clustering of the organelles, which closely resembled the effect of GFP-BICD2N^{MTS} (Fig. 1D-E). Treatment with the microtubule depolymerizing agent nocodazole significantly reduced the perinuclear accumulation of mitochondria observed in GFP-ScaC^{MTS} cells, confirming that ScaC-induced clustering relies on intact microtubules (Supplementary Fig. 1E-F).

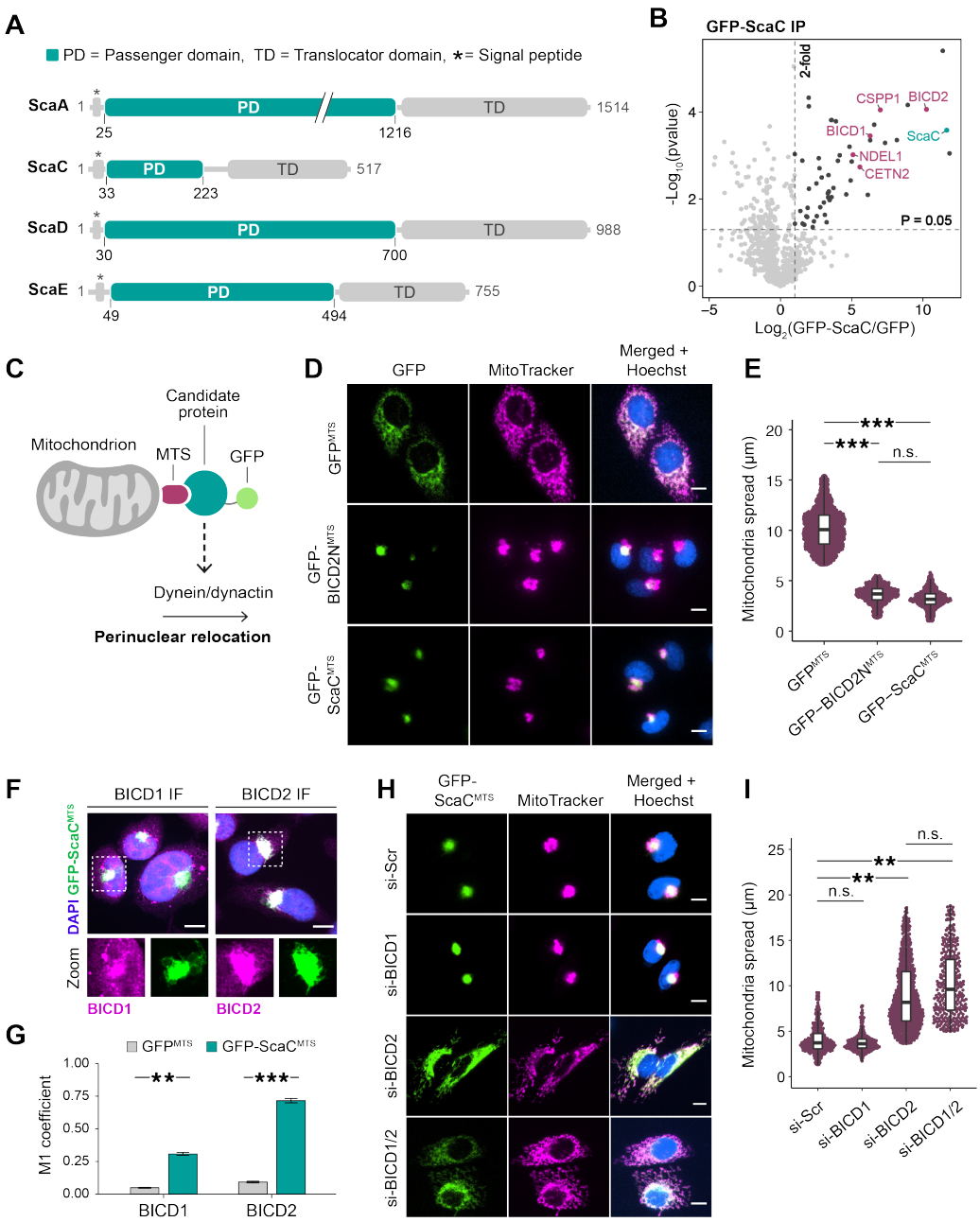

Figure 1. The bacterial protein ScaC recruits the activating adaptors BICD1 and BICD2. (A) Domain architecture of conserved Sca proteins. The passenger domains are highlighted in teal. **(B)** Volcano plot summarising the results of GFP-ScaC co-IP/MS in HeLa Flp-In cells. The significant enrichment levels were calculated from n=3 independent replicates. GFP-ScaC is highlighted in teal. Proteins with known links to microtubules are indicated in magenta. **(C)** Visual schematic of mitochondrial relocation assay. **(D)** Representative images of mitochondrial relocation assay with GFP^{MTS}, GFP-BICD2N^{MTS} and GFP-ScaC^{MTS} cell lines. Scale bars indicate 10 µm. **(E)** Quantification of mitochondrial spread for GFP^{MTS}, GFP-BICD2N^{MTS} and GFP-ScaC^{MTS} samples. P-values were calculated from n=3 independent replicates using two-tailed ANOVA (F value = 92.585) with a Tukey HSD post-hoc test. ***= p<0.001. **(F)** Representative IF images showing colocalization of GFP-ScaC^{MTS} with BICD1 and BICD2 respectively. Scale bars indicate 10 µm. **(G)** Barplot showing colocalization of BICD1 and BICD2 with GFP^{MTS} (grey) or GFP-ScaC^{MTS} (teal). Colocalization was measured using the Manders coefficient (M1). P-values were calculated from n=3 independent replicates using a two-tailed T-test. Error bars indicate mean ± standard error. **=p<0.01, ***=p<0.001. **(H)** Representative images of GFP-ScaC^{MTS} cells treated with siRNAs against BICD1 and/or BICD2. A scrambled siRNA (si-Scr) was used as a negative control. Scale bars indicate 10 µm. **(I)** Quantification of mitochondrial spread in siRNA-treated GFP-ScaC^{MTS} cells. P-values were calculated from n=3 independent replicates using two-tailed ANOVA (F value = 19.794) with a Tukey HSD post-hoc test. **=p<0.01.

Our pull-down experiments indicated an interaction between ScaC and the activating adaptors BICD1 and BICD2 (Fig. 1B). Accordingly, immunofluorescence analysis of GFP^{MTS} and GFP-ScaC^{MTS} cells showed that BICD1 and BICD2 are both recruited to mitochondrial clusters in a ScaC-dependent manner (Fig. 1F-G, Supplementary Fig. 1G). To determine if ScaC requires BICD1 and BICD2 for mitochondrial relocation, we performed knockdowns of both adaptors in GFP-ScaC^{MTS} cells (Fig. 1H-I, Supplementary Fig. 1H). Depletion of BICD1 alone did not affect the ScaC-dependent clustering of mitochondria. However, knockdown of BICD2 strongly inhibited mitochondrial accumulation at the perinuclear region, and a similar phenotype was observed when a double BICD1/2 knockdown was performed. Notably, the effect of BICD2 knockdown on mitochondrial distribution was specific to GFP-ScaC^{MTS} cells, and was not observed in control GFP^{MTS} lines (Supplementary Fig. 1I-J). Based on these results, we conclude that BICD2, rather than BICD1, acts as the predominant adaptor in our cell-based system. The gene expression levels of *BICD2*, measured by qPCR, are ~57-fold higher than those of *BICD1* in our cell model (Supplementary Fig. 1K), which suggests that BICD2 is highly abundant and therefore able to compensate for BICD1 depletion.

BICD2 is required for efficient perinuclear translocation of *O. tsutsugamushi*

Since the ScaC-BICD2 interaction is sufficient to elicit microtubule-based transport in cells, we asked whether it is required for *O. tsutsugamushi* motility during infection. Because *O. tsutsugamushi* is genetically intractable, we were unable to perform knockout experiments for ScaC. Instead, we carried out siRNA-mediated knockdowns of BICD1 and BICD2 and determined the effect on bacterial localization. *O. tsutsugamushi* was used to infect HeLa ATCC cells at multiplicity of infection (MOI) 50:1, and bacterial localization was assessed at 24 hours post-infection (hpi) by immunofluorescence (Fig. 2A-C). Similar to

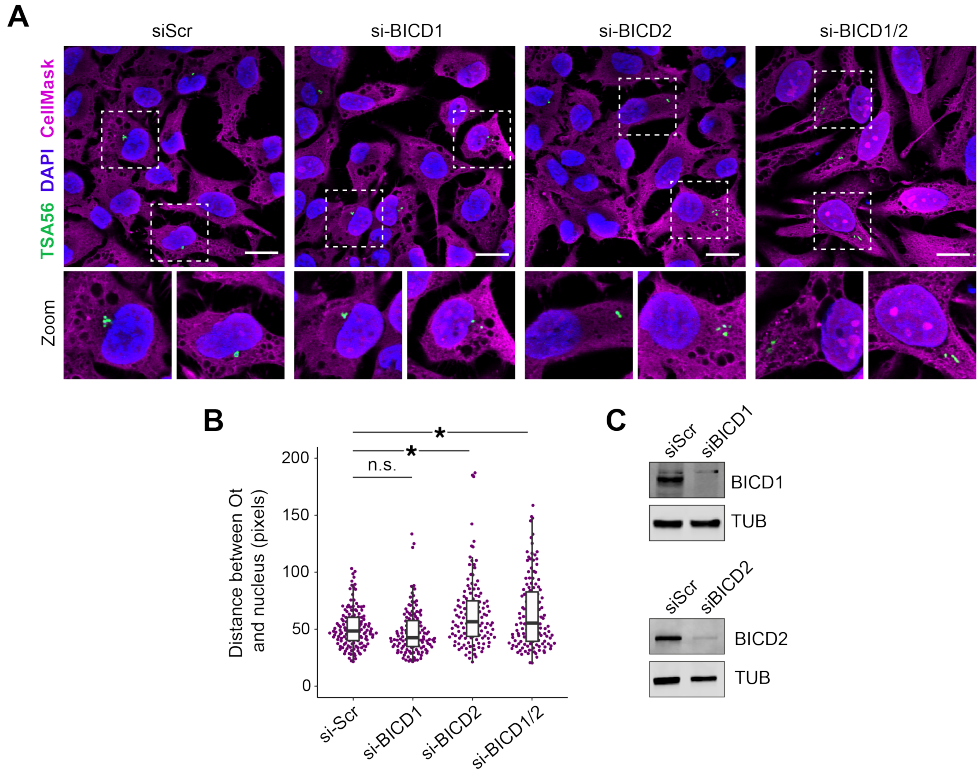

Figure 2. BICD2 is required for perinuclear translocation of O. tsutsugamushi. (A) Representative IF images showing localization of *O. tustsugamushi* (green) at 24 hpi in HeLa ATCC cells treated with siRNAs against BICD1 and/or BICD2. A scrambled siRNA (si-Scr) was used as a negative control. Cytosol and nuclei were stained with CellMask and DAPI respectively. Scale bars represent 20 µm. **(B)** Quantification of the pixel distance between bacteria and the nucleus in siRNA-treated HeLa ATCC cells. P-values were calculated from n=3 independent replicates using two-tailed ANOVA (F value = 10.948) with a Tukey HSD post-hoc test. *=p<0.05. **(C)** Western blots showing knockdown of BICD1 and BICD2 upon siRNA treatment. B-tubulin was used as a loading control.

our mitochondrial relocation assay, knockdown of BICD1 had no effect on bacterial translocation. However, depletion of either BICD2 alone or BICD1 and BICD2 together significantly decreased perinuclear clustering of *O. tsutsugamushi*. (Fig. 2A-B).

ScaC interacts with the CC3 domain of BICD2

To determine whether ScaC recruits BICD2 directly, we purified both proteins and tested their ability to form a complex in vitro. Circular dichroism spectroscopy showed that the ScaC passenger domain adopts a classical α-helical conformation (Supplementary Fig. 2A). Similar to BICD2[29], ScaC behaves as a dimer in solution (Supplementary Fig. 2B-C), consistent with its predicted coiled-coil structure (Supplementary Fig. 2D). Size exclusion chromatography showed that ScaC and BICD2 form a stoichiometric complex, indicating that they do not require additional factors to interact (Fig. 3A). SEC-MALS analysis estimated a complex mass of 244 kDa which is consistent with a ScaC-BICD2 complex of 2:2 stoichiometry (Fig. 3B).

To identify the ScaC-binding region on BICD2, we designed four BICD2 truncations and tested their ability to interact with ScaC (Fig. 3C, Supplementary Fig. 2E). ScaC bound to the C-terminus of BICD2 ($BICD^{342-800}$ or BICD2C) but not to the N-terminus ($BICD2^{1-400}$ or BICD2N). Furthermore, we found that the third C-terminal coiled-coil domain (CC3) of BICD2 ($BICD2^{711-800}$) was both necessary and sufficient for the interaction with ScaC (Fig. 3C, Supplementary Fig. 2E). These findings were validated by cross-linking mass spectrometry of purified ScaC and BICD2 with the zero-length cross-linker EDC, which showed an enrichment of cross-links around the CC3 of BICD2 (Fig. 3D, Supplementary Table 5). The CC3 cross-links converged on the central region of the ScaC passenger domain, (residues 119-136), suggesting it contains the binding site for BICD2. In line with this observation, a truncated fragment of ScaC spanning residues 50-159 retained the ability to bind BICD2 (Fig. 3E). ScaC was also able to bind the CC3 of BICD1, which shares 94% homology to the CC3 of BICD2, suggesting that a shared mechanism underlies both interactions (Supplementary Fig. 2F).

ScaC has evolved a novel interface for BICD2 binding

The host proteins RAB6 and RANBP2 also interact with the CC3 domain of BICD2 to facilitate the transport of their associated cargoes (Supplementary Fig. 3A)[29-31]. RAB6 is a small GTPase protein which orchestrates the retrograde movement of Golgi-derived and secretory vesicles[31,32], whereas the nucleoporin RANBP2 recruits dynein motors to the nuclear envelope to drive separation of the nucleus from the centrosomes during G2 phase[30]. Although these two effectors employ similar mechanisms for mediating transport, they bind non-overlapping sites on BICD2 (Fig. 3F, Supplementary Fig. 3A-B)[33]. We set out to determine whether ScaC binds BICD2 via one of these sites or uses a novel binding interface. To this end, we introduced mutations at two residues in the CC3 domain of BICD2, L742 and L786, which are essential for the interaction with RANBP2 and RAB6, respectively (Fig. 3F)[29,33]. To validate our mutants, we purified a RANBP2 fragment (residues 2148-2240 or $RANBP2^{min}$), which contains the minimal BICD2 binding domain[34,35], and a GTP-locked RAB6 mutant ($RAB6^{Q72L}$). As anticipated, the L742A mutation resulted in loss of RANBP2 binding in an in vitro pulldown assay, while the L786A mutation prevented $RAB6^{Q72L}$ binding. A double L742A/L786A mutant effectively abolished the interaction with both proteins (Fig. 3G). In contrast, we found that ScaC retained the ability to bind all mutant versions of BICD2, suggesting that it binds the adaptor in a different way (Fig. 3G). This is consistent with the observation that ScaC does not bind BICDR1, another member of the Bicaudal D family which retains the conserved Rab6 binding site (Supplementary Fig. 3C-D)[36]. Finally, we performed a competition pull-down assay to determine whether the ScaC binding site overlaps with those of RANBP2 or RAB6. In the presence of ScaC, RAB6 binding to BICD2 was decreased by 60% while RANBP2 binding was fully abrogated (Fig. 3H-I). This hints that ScaC occupies a region on BICD2 which broadly overlaps with the RANBP2 binding region and at least partially extends to the RAB6 interaction site.

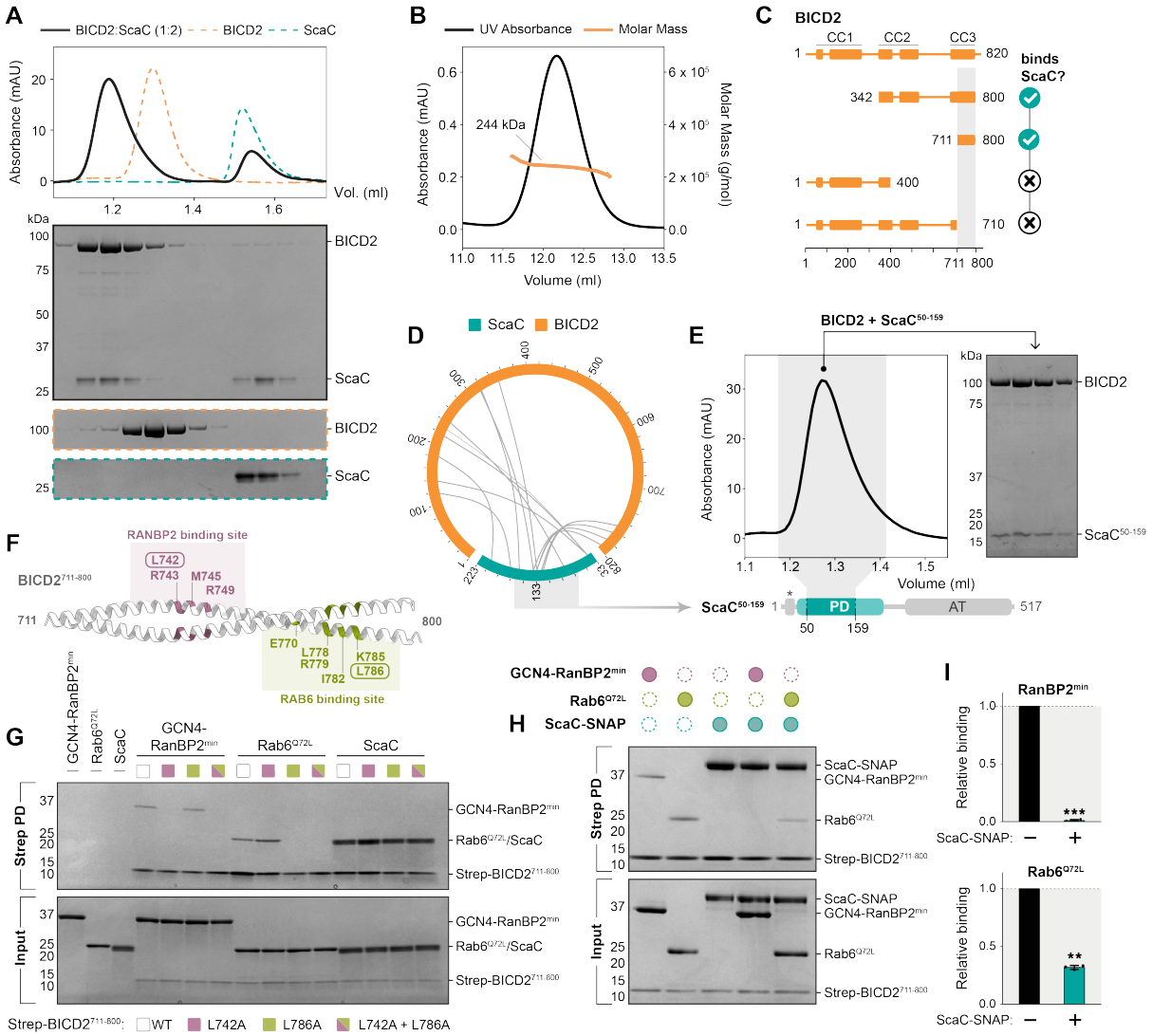

Figure 3. ScaC binds the C-terminus of BICD2 through a novel interface. **(A)** Chromatogram for the BICD2-ScaC complex (black). Purified BICD2 and ScaC were mixed in 1:2 molar ratio. Individual traces for BICD2 (orange) and ScaC (green) are shown. SDS-PAGE gels show fractions underlying the relevant protein peaks. **(B)** SEC-MALS for the BICD2-ScaC complex. The molar mass of the complex is indicated. **(C)** Schematic diagram showing mapping of the ScaC-binding domain (highlighted in grey) using BICD2 truncations. **(D)** Cross-linking/MS of purified BICD2-ScaC complexes using ECD. Heteromeric cross-links are shown. **(E)** Chromatogram of the BICD2-ScaC$^{59-159}$ complex. The SDS-PAGE gel shows fractions underlying the complex peak. **(F)** AlphaFold prediction of BICD2$^{711-800}$. The previously experimentally validated residues involved in RANBP2 and RAB6 binding are highlighted in pink and green respectively. **(G)** SDS-PAGE gels showing in vitro pull-downs of different Strep-BICD2$^{711-800}$ mutants in the presence of 3.5-fold excess GCN4-RnaBP2^{min}, Rab6^{Q72L} or ScaC. **(H)** Competition pull-down assay using Strep-BICD2$^{711-800}$ in the presence of different combinations of GCN4-RnaBP2^{min}, Rab6^{Q72L} and ScaC-SNAP. **(I)** Quantification of GCN4-RnaBP2^{min} (top) and Rab6^{Q72L} (bottom) binding to Strep-BICD2$^{711-800}$ in the absence or presence of ScaC-SNAP. P-values were calculated from n=3 independent replicates using a two-tailed T- test. **=p<0.01, ***=p<0.001.

ScaC activates BICD2 for dynein motility

In the absence of a suitable cargo, BICD2 undergoes autoinhibition by folding of the C-terminal domain over the N-terminus, which effectively blocks the recruitment of dynein and dynactin[24,37]. To investigate whether ScaC binding to BICD2 is sufficient to relieve autoinhibition, we purified BICD2N and BICD2C constructs, which form a complex (Fig. 4A) as reported previously[24,33]. ScaC binding to BICD2C prevented the association

with BICD2N, suggesting that ScaC displaces the N-terminus of BICD2 to promote an active open conformation (Fig. 4A). To confirm this process is sufficient to stimulate dynein motility, we used single-molecule fluorescence microscopy to monitor the movement of TMR-labelled dynein along microtubules (Fig. 4B-C). In the presence of dynactin and the constitutively active cargo adaptor BICD2N (DDB^N), dynein displayed robust directional movement. Conversely, full-length BICD2 produced fewer processive complexes (DDB), consistent with previous reports[38,39] (Fig. 4B-C). Adding ScaC to full-length BICD2 (DDBS) increased the number of processive events by 3-fold (for an average of 1.22±0.12 vs. 0.44±0.12 processive events/µm MT/min). Importantly, the increase in dynein motility caused by ScaC was BICD2-dependent, since DDS only exhibited diffusive movement along microtubules (Figure 4B-C). We did not observe any significant differences in velocity or run length between DDBS and DDB conditions, with average speeds ranging between 0.9 and 1.3 µm s^{-1} and run lengths between 6.2 and 8.7 µm (Supplementary Fig. 4A-B). To verify that ScaC co-migrates with the active complex following BICD2 activation, we performed dual colour motility assays with ScaC-AF647 and TMR-dynein. We found that 74.8±3.2% of moving dyneins colocalized with ScaC in DDBS complexes, thus demonstrating that ScaC is co-transported with the motile machinery (Fig. 4D). Similarly, colocalization was observed for ScaC-AF647 and BICD2-AF488 (Supplementary Fig. 4C). Overall, our data point toward a model whereby ScaC actively promotes bacterial transport by opening up BICD adaptors for dynein and dynactin recruitment (Fig. 5).

DISCUSSION

Many cytosolic bacteria, including *Listeria* and certain *Rickettsia* species, move intracellularly by polymerizing actin tails on their surface[22,40-42]. Despite belonging to the Rickettsiaceae family, *O. tsutsugamushi* lacks this ability[2], and has instead developed a mechanism to directly engage the dynein

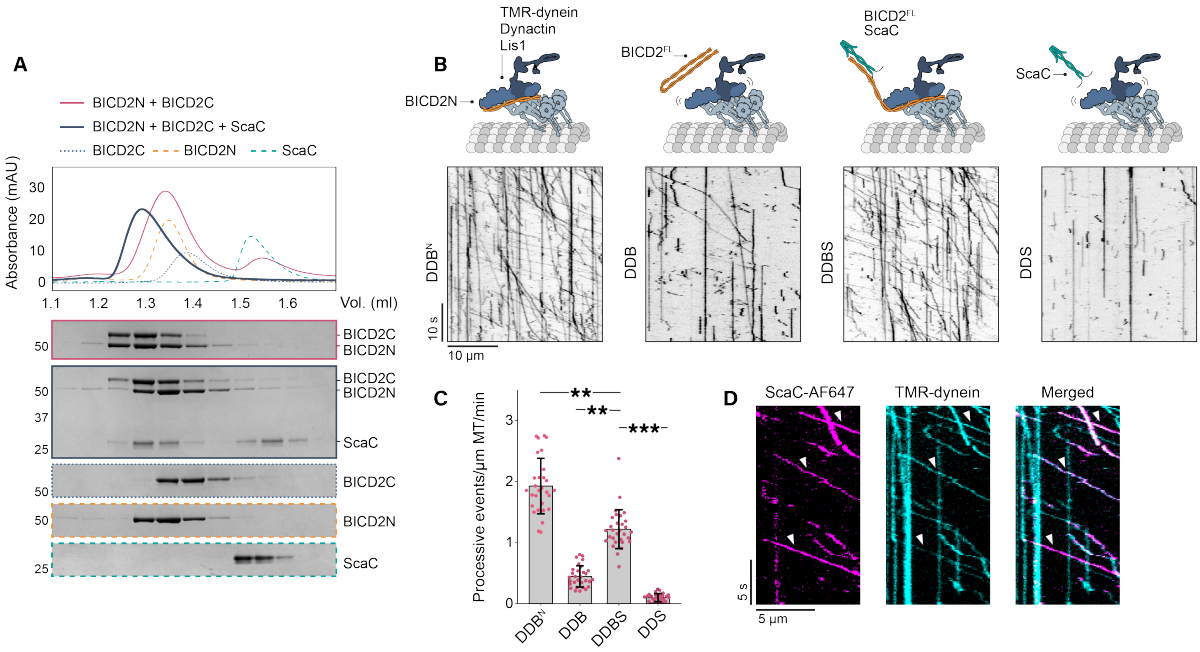

Figure 4. ScaC activates BICD2 for dynein motility. (A) Chromatograms showing disruption of the BICD2N-BICD2C complex upon BICD2C binding to ScaC. Individuals traces for BICD2N, BICD2C and ScaC are shown. SDS-PAGE gels show fractions underlying the relevant protein peaks. **(B)** Representative kymographs of TMR-dynein mixed with dynactin and Lis1 in the presence of either BICD2N, full-length BICD2, full-length BICD2 and ScaC or ScaC only. **(C)** Barplot showing the number of processive events per microtubule µm per minute for different complex combinations (as in B). P-values were calculated from n=3 independent replicates using two-tailed ANOVA (F value = 52.532) with a Tukey HSD post-hoc test. Error bars indicate mean ± standard deviation. **=p<0.01, ***=p<0.001. **(D)** Representative kymographs showing colocalization of Scac-AF674 (magenta) and TMR-dynein (cyan). Arrows indicate colocalization events. Scale bars are shown.

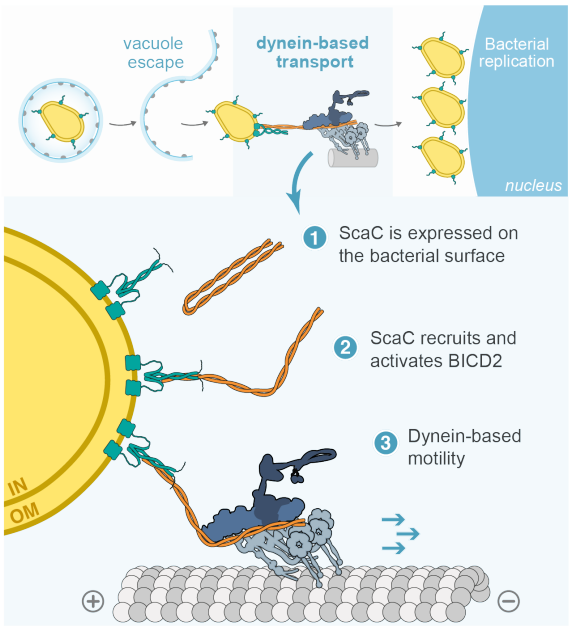

Figure 5. Model of *O. tsutsugamushi* transport by ScaC and BICD2. Following vacuole escape, *O. tsutsugamushi* hijacks the adaptor protein BICD2 to undergo microtubule- and dynein-based transport to the perinuclear region, where it establishes a replicative niche. In molecular detail: (1) the autotransporter protein ScaC, which forms a dimer on the bacterial outer membrane, recruits the activating adaptor BICD2 to the bacterial surface. (2) Binding of ScaC to the C-terminus of BICD2 relieves the adaptor from autoinhibition. (3) Activated BICD2 is able to form a complex with dynein and dynactin, initiating movement along microtubules. IN = inner membrane, OM = outer membrane.

machinery for intracellular transport[2] (Fig. 5). Microtubule-based movement has been observed for another cytosolic bacterium, *Actinobacillus actinomycetemcomitans,* which spreads to adjacent cells via microtubule-containing protrusions[43]. However, *A. actinomycetemcomitans* motility is directed towards the plus ends of microtubules[43] suggesting that it involves kinesin motors.

The exact purpose of dynein-based transport within the *O. tsutsugamushi* lifecycle remains enigmatic. It is possible that the perinucleus provides a favourable environment for bacterial growth. This appears to be the case for *Chlamydia trachomatis*, which resides in a vacuole and uses dynein to positions itself near the nucleus to acquire sphingolipids from the Golgi[44]. Another possibility is that *O. tsutsugamushi* exploits dynein to evade host defences. It is known for example that *Listeria* species use actin-based motility to avoid recognition by the host autophagy machinery[42], which is recruited to damaged vesicles upon phagosomal escape[45]. Given that *O. tsutsugamushi* also breaks out of its vacuole to enter the cytosol, dynein-driven movement could provide a way to quickly retreat from the site of autophagosome formation.

Among the five Sca proteins found in *O. tsutsugamushi* strains, ScaC displays the highest degree of conservation in its passenger domain, underscoring its importance for infection[19]. Previous studies have implicated ScaC in bacterial adhesion to host cells through interaction with the fibronectin receptor, although this process is not sufficient to induce entry on its own[19]. Here, we show that ScaC plays an additional role immediately after cell entry, mediating bacterial movement along microtubules to the perinucleus, where bacterial replication occurs. It was recently shown that during infection of L929 and HUVEC cells ScaC levels are higher in extracellular bacteria than intracellular bacteria[11]. This expression pattern is consistent with ScaC participating in key processes during the early phases of infection, and its downregulation could provide a mechanism for the bacterium to release dynein and return to the cell periphery for budding after replication has taken place.

In this study, we show that ScaC engages the host adaptor protein BICD2 and that this interaction is important for motility. Although BICD1 can also interact with ScaC, its depletion did not produce a phenotype in our cell-based assays, likely due to functional redundancy. We conclude that BICD2 is the predominant adaptor in epithelial cells, although it is possible that BICD1 plays a larger role in other cell types targeted by *O. tsutsugamushi* where it is expressed more abundantly, such as lymphatic endothelial cells[46]. Beyond its physiological roles in the transport of secretory vesicles and maintaining nuclear positioning, BICD2 is reported to be hijacked by viruses such as HIV-1 and HSV-1, which undergo retrograde transport to the host cell nucleus[47,48]. This suggests multiple pathogens have evolved the ability to exploit this specific adaptor, although our study provides the first example of BICD2 manipulation by a bacterium. We

show that ScaC binds the C-terminal CC3 domain of BICD2 to relieve the adaptor from autoinhibition. A similar mechanism had initially been proposed for HIV-1, as purified viral capsids were found to interact with the BICD2 CC3[47,49]. However, recent reports suggest that HIV-1 binds directly to the dynein tail and is able to hitchhike on dynein/dynactin complexes bound to various adaptors[50]. This approach is remarkably different from the strategy employed by *O. tsutsugamushi*, where association with dynein occurs via a specific cargo-adaptor interaction.

The CC3 domain of BICD2 is known to harbour the binding sites for other conserved host cargoes[29-31]. However, the way ScaC binds BICD2 differs from both RAB6 and RANBP2, reinforcing the notion that BICD2 autoinhibition can be overcome through cargo binding at multiple sites within the CC3 domain[38,39]. Furthermore, ScaC was able to outcompete RANBP2 and, to some extent, RAB6 for BICD2 binding, indicating that it has evolved a higher affinity for BICD2 compared to its host counterparts. This adaptation seems logical, as unlike endogenous cargoes, which require a degree of flexibility to ensure timely and reversible transport, *O. tsutsugamushi* would likely benefit from securing a robust interaction with BICD2 to move quickly and efficiently within its host cell. We found that the soluble domain of ScaC forms a coiled coil in vitro, suggesting a mechanism where the passenger domains of two neighbouring ScaC molecules interact with each other after translocation across the outer membrane. We show that ScaC and BICD2 bind with 2:2 stoichiometry, similar to other BICD2-cargo complexes[29,34,35,51]. In the case of RAB6, it is thought that two monomers bind symmetrically on both faces of BICD2[29], whereas RANBP2 has been suggested to bind as a dimer to a single site on BICD2[39]. The latter model could be explained by a high degree of asymmetry in the CC3 domain which would cause the two faces of BICD2 to be structurally distinct, as revealed by a crystal structure of BicD (the *Drosophila* homolog of BICD2)[29]. The dimeric nature of ScaC suggests that is also binds asymmetrically on one side of BICD2. However, it is also possible that the ScaC coiled coil undergoes partial or complete dissociation, allowing each monomer to independently bind a face of BICD2.

Taken together, our findings describe a novel pathway for bacterial transport in molecular detail and lay the groundwork for further research into how perinuclear transport affects the *O. tsutsugamushi* lifecycle.

MATERIALS AND METHODS

Constructs and plasmids

The full-length mouse BICD2 sequence (UniProt Q921C5) was codon optimized for expression in Sf9 insect cells (Epoch Life Sciences) and cloned into a pACEBac1 vector encoding a N-terminal Strep-tag followed a PreScission (Psc) protease cleavage site (pACEBac1-Strep-Psc). BICD2 truncations 1-400 (BICD2N), 342-800 (BICD2C), 342-541 (BICD2$^{342-541}$), 711-800 (BICD2$^{711-800}$) and 1-710 (BICD2$^{1-710}$) were subcloned into pACEBac1-Strep-Psc. BICD2-SNAP was cloned by insertion of a SNAP tag to the C-terminus of full-length BICD2 in a pACEBac1-Strep-Psc backbone. L742A and L786A mutations were inserted into pACEBac1-Strep-Psc-BICD2$^{711-800}$ (either individually or in combination) by site-directed mutagenesis using the Q5 Site-Directed Mutagenesis Kit (NEB). The full-length mouse BICD1 sequence (UniProt Q8BR07) was synthesized by Twist Biosciences, and residues 713-802 were subcloned into pACEBac1-Strep-Psc.

The passenger domain sequences of ScaA (residues 25-1216), ScaC (residues 33-223), ScaD (residues 30-700) and ScaE (residues 49-494) were synthesized by Epoch Life Sciences and cloned into a pCDNA5/FRT/TO vector fused to a N-terminal eGFP tag. GFP^{MTS} and GFP-BICD2N^{MTS} plasmids were previously described[26]. GFP-ScaC^{MTS} was cloned by addition of a C-terminal MTS tag to the pCDNA5/FRT/TO-eGFP-ScaC plasmid. For bacterial expression of ScaC, the passenger domain was subcloned into a pET22b vector encoding a C-terminal TEV-6His cassette. To generate a ScaC-SNAP construct, a SNAP tag was fused to the C-terminus of ScaC in pET22b-ScaC-TEV-6His. ScaC$^{50-159}$ was subcloned into a pET28 vector encoding a N-terminal Strep-Psc cassette.

The full-length human RANBP2 sequence was codon optimized for expression in Sf9 insect cells (Epoch Life Sciences). Residues 2148-2240 fused to a N-terminal GCN4 dimerization tag were subcloned into a pACEBac1 vector with a N-terminal 6xHis-ZZ tag followed by a TEV cleavage site. The human RAB6^{Q72L} was subcloned from Addgene plasmid #49483 into a bacteria expression pGEX-4T-1 vector encoding a N-terminal GST tag followed by a TEV cleavage site.

Full-length human LIS1 was expressed from a previously described pFastbac-ZZ-TEV-LIS1 plasmid[26]. For expression of SNAP-tagged full-length human dynein, a previously described pDyn3 plasmid (Addgene #64069) was used[16].

Cell lines

HeLa Flp-In cell lines (GFP, GFP-ScaA, GFP-ScaC, GFP-ScaD, GFP-ScaE, GFP^{MTS}, GFP-BICD2N^{MTS} and GFP-ScaC^{MTS}) were generated using the FLP-FRT recombination system as previously described[26]. In brief, Flp-In T-REX HeLa cells were transfected with 1.8 µg of pOGG4 plasmid and 200 ng of pcDNA5/FRT/TO plasmid encoding the relevant transgene cassette using FuGENE HD transfection reagent (Promega). Cells with a stably integrated transgene were selected with 150 µg/mL hygromycin for 4-5 days. Cells were maintained in DMEM (Gibco) supplemented with 10% FBS and 1% penicillin streptomycin. Transgene expression was induced by adding 10 µg/mL tetracycline to the culture medium. HeLa ATCC CCL-2 cells were cultured in DMEM (41965-039, Gibco) supplemented with 10% FBS. All cells were maintained at 37˚C and 5% CO_2 atmosphere.

Protein expression

For bacterial expression of recombinant proteins, SoluBL21 *E. coli* cells transformed with the expression plasmid were grown to O.D. 0.6-0.8 and induced with 500 mM IPTG. Expression was carried out at 25˚C for 14 hours in a shaking bacterial incubator (speed 180 rpm). Pellets were harvested by centrifugation at 4,000 rcf for 20 minutes at 4˚C, followed by flash-freezing and long-term storage at -80˚C.

For insect cell expression, protein constructs were cloned in pACEBac1 vectors and transformed into EmBacY *E. coli* cells. 4 µg of purified bacmid DNA were transfected into $1x10^6$ Sf9 cells in a well of a 6-well plate using 6 µL of FuGENE HD transfection reagent (Promega). After 7 days of incubation at 27˚C, 1 mL of baculovirus-containing medium was used to infect 50 mL of Sf9 cells at a density of $1x10^6$ cells/mL to generate P2 virus. P2 cultures were incubated at 27˚C for 5 days in a shaking incubator. The P2 virus was harvested by collecting the supernatant after centrifugation at 3,000 rcf for 10 minutes and was stored at 4˚C. For expression, 10 mL of P2 virus were used to infect 1L of Sf9 cells at a density of $1.5\text{-}2x10^6$ cells/mL for 72 hours at 27˚C in a shaking incubator. Pellets were harvested by centrifugation at 4,000 rcf for 20 minutes at 4˚C, followed by flash-freezing and long-term storage at -80˚C.

Protein purification

All BICD2 and BICD1 constructs were expressed in Sf9 insect cells. Pellets from 1L of expression culture were resuspended in 45 mL lysis buffer (30 mM HEPES pH 7.2, 300 mM NaCl, 1mM DTT, 2mM PMSF) supplemented with 1 cOmplete-EDTA protease-inhibitor tablet (Sigma-Aldrich) and lysed using a Dounce tissue homogenizer with 20-25 strokes. Lysates were cleared by centrifugation at 35,000 rcf for 45 minutes at 4˚C followed by filtering with a GF filter (Sartorius). Cleared lysates were then incubated with 1.5 mL of StrepTactin Sepharose beads (IBA Lifesciences) for 1 hour at 4˚C on a rotator. Beads were washed on a gravity column with 200 mL wash buffer (30 mM HEPES pH 7.2, 300 mM NaCl, 1mM DTT), and Strep-tagged proteins were eluted with 5-7 mL of wash buffer supplemented with 3 mM desthiobiotin. For AF488-labelled BICD2-SNAP, beads were incubated with 10 µM SNAP-Surface Alexa Fluor 488 (NEB) for 1 hour at 4˚C prior to elution. Eluted proteins were concentrated to a volume of ~0.5 mL and loaded onto a Superose 6 Increase 10/300 column (Cytiva) pre-equilibrated in GF150 buffer (25 mM HEPES pH 7.5, 150 mM KCl, 1 mM $MgCl_2$, 1 mM DTT). Peak fractions were pooled and concentrated to 1.5-6 mg/mL, depending on the specific construct. Concentrated proteins were flash-frozen and stored at -80˚C.

For purification of GCN4-RANBP2^{min}, a pellet from 1L of Sf9 insect cell expression culture was resuspended in 45 mL lysis buffer (200 mM Tris-HCl pH 8, 300 mM NaCl, 20 mM Imidazole, 1 mM DTT, 2 mM PMSF). supplemented with 1 cOmplete-EDTA protease-inhibitor tablet (Sigma-Aldrich) and lysed using a Dounce tissue homogenizer with 20-25 strokes. The lysate was cleared by centrifugation at 35,000 rcf for 45 minutes at 4˚C followed by filtering with a GF filter (Sartorius). The cleared lysate was incubated with 2 mL Ni-NTA agarose (Qiagen) on a rotator for 1 hour at 4˚C. Beads were washed on a gravity column with 200 mL wash buffer (20 mM Tris-HCl pH 8, 300 mM NaCl, 20 mM Imidazole, 1mM DTT), and His-tagged proteins were eluted with 5-7 mL of elution buffer (20 mM Tris-HCl pH 8, 300 mM NaCl, 200 mM Imidazole, 1mM DTT). The eluted proteins were dialysed overnight in 20 mM Tris-HCl buffer (pH 8) supplemented with 1 mM DTT using a 10 kDa MWCO SnakeSkin dialysis tube (ThermoFisher), then concentrated to ~0.5 mL and loaded onto a Superose 6 Increase 10/300 column pre-equilibrated in GF150 buffer. Peak fractions were pooled and concentrated to 7.5 mg/mL, flash-frozen and stored at -80˚C.

ScaC, ScaC-SNAP and Sca$C^{50\text{-}159}$ were expressed in SoluBL21 *E. coli* cells. Pellets from 1L of expression culture were resuspended in 45 mL lysis buffer (20 mM Tris-HCl pH 8, 300 mM NaCl, 20 mM Imidazole, 1mM DTT, 2mM PMSF, 0.3% Triton-X-100) supplemented with 1 cOmplete-EDTA protease-inhibitor tablet (Sigma-Aldrich) and lysed by sonication (3 minutes, 70% amplitude, pulse: 3s on, 7s off) at 4˚C. Lysates were cleared by centrifugation at 35,000 rcf for 30 minutes at 4˚C followed by filtering with a GF filter (Sartorius). For purification of ScaC and ScaC-SNAP, cleared lysates were incubated with 2 mL Ni-NTA agarose (Qiagen) on a rotator for 1 hour at 4˚C. Beads were washed on a gravity column with 200 mL wash buffer (20 mM Tris-HCl pH 8, 300 mM NaCl, 20 mM Imidazole, 1mM DTT, 10 mM $MgCl_2$, 1 mM ATP), and His-tagged proteins were eluted with 5-7 mL of elution buffer (20 mM Tris-HCl pH 8, 300 mM NaCl, 200 mM Imidazole, 1mM DTT). The eluted proteins were dialysed overnight in 20 mM Tris-HCl buffer (pH 8) supplemented with 1 mM DTT using a 10 kDa MWCO SnakeSkin dialysis tube (ThermoFisher) and loaded onto a MonoQ 5/50 GL column for anion exchange chromatography. For purification of Sca$C^{50\text{-}159}$, the cleared lysate was incubated with 1.5 mL StrepTactin Sepharose beads (IBA Lifesciences) for 1 hour at 4˚C on a rotator. Beads were washed on a gravity column with 200 mL wash buffer (30 mM

HEPES pH 7.2, 300 mM NaCl, 1mM DTT, 10 mM $MgCl_2$, 1 mM ATP), and Strep-tagged proteins were eluted with 5-7 mL of wash buffer supplemented with 3 mM desthiobiotin. For all ScaC constructs, peak fractions were concentrated to ~0.5 mL and loaded onto a Superdex 200 Increase 10/300 column pre-equilibrated in GF150 buffer. Peak fractions were pooled and concentrated to 2-3 mg/mL, flash-frozen and stored at -80˚C. For AF647-labelled ScaC-SNAP, the protein eluted from MonoQ 5/50 GL was incubated with 10 µM SNAP-Surface Alexa Fluor 647 (NEB) for 1 hour at 4˚C prior to gel filtration.

For purification of $RAB6^{Q72L}$, a pellet from 1L of SoluBL21 *E. coli* cell expression culture was resuspended in 45 mL lysis buffer (PBS, 5 mM DTT, 1 mM PMSF, 0.5% Triton-X 100, 10% glycerol, 10 µM GTP) and lysed by sonication (70% amplitude, 2 minutes, pulse: 2s on 12s off) at 4˚C. The lysate was cleared by centrifugation at 35,000 rcf for 30 minutes at 4˚C followed by filtering with a GF filter (Sartorius). The cleared lysate was incubated with 3 mL of Glutathione Sepharose 4B resin (Cytiva) supplemented with 10 µM GTP at 4˚C on a rotator for 2 hours. The resin was washed with 450 mL of PBS with 10% glycerol and incubated overnight with 35 µL (35 units) thrombin solution at room temperature for cleavage of the GST tag. Cleaved proteins were separated from the resin using a gravity column, concentrated to ~0.5 mL and loaded onto a Superose 6 Increase 10/300 column pre-equilibrated in GF150 buffer supplemented with 10 µM GTP. Peak fractions were pooled and concentrated to 7 mg/mL, flash-frozen and stored at -80˚C.

Dynein was purified from Sf9 insect cells as previously described[16]. In brief, a pellet from 1L of expression culture was resuspended in 45 mL lysis buffer (50 mM HEPES pH 7.2, 100 mM NaCl, 10% glycerol, 1 mM DTT and 100 µM ATP, 2 mM PMSF) supplemented with 1 cOmplete-EDTA protease-inhibitor tablet (Sigma-Aldrich) and lysed using a Dounce tissue homogenizer with 30 strokes. The lysate was cleared by centrifugation at 70,000 rcf for 45 minutes at 4˚C followed by filtering with a GF filter (Sartorius). The cleared lysate was incubated with 4 mL of IgG beads (Cytiva) at 4˚C on a rotator for 4 hours. The beads were washed with 150 mL wash buffer (50 mM HEPES pH 7.2, 100 mM NaCl, 10% glycerol, 1 mM DTT and 100 µM ATP) and incubated with 10 µM SNAP-Cell TMR-Star dye (NEB) for 1 hour at 4˚C. The beads were then transferred to a gravity column and washed with 100 mL of TEV Buffer (50 mM Tris-HCl pH 7.4, 150 mM KAc, 2 mM MgAc, 1 mM EGTA, 10% (v/v) glycerol, 0.1 mM ATP, 1 mM DTT). The protein was cleaved from the beads by overnight incubation with 400 µg of TEV protease at 4˚C. The flowthrough containing the cleaved protein was collected and concentrated to ~2 mg/mL, then loaded onto a TSKgel G4000SWXL column pre-equilibrated with GF150 buffer supplemented with 0.1 mM ATP. Peak fractions were pooled and concentrated to 2 mg/mL. The concentrated protein was supplemented with 10% glycerol, flash-frozen and stored at -80˚C.

Dynactin[16] and Lis1[26] were expressed and purified as described previously.

Co-IP mass spectrometry

HeLa Flp-In cells expressing either GFP, GFP-ScaA, GFP-ScaC, GFP-ScaD or GFP-ScaE transgenes were grown to confluence in a 15-cm tissue culture dish in the presence of 10 µg/mL tetracycline. Cells were detached using 0.25% trypsin-EDTA solution (ThermoFisher) and pellets were washed twice with PBS. Pellets were lysed with co-IP lysis buffer (10 mM Tris pH 7.5, 150 mM NaCl, 0.5 mM EDTA, 0.5% NP-40, protease inhibitor, 1 mM PMSF) on ice for 30 minutes, and lysates were cleared by centrifugation at 15,000 rcf at 4˚C for 15 minutes. Protein concentrations were measured by Bradford assay. Samples were diluted to 4 mg/mL with dilution buffer (10 mM Tris pH 7.5, 150 mM NaCl, 0.5 mM EDTA), and 500 µL were incubated with 25 µL of magnetic GFP-trap beads (Chromotek) for 1 hour at 4˚C on a rotator (speed 5 rpm). The beads were washed three times with 500 µL dilution buffer followed by buffer exchange with 100 mM ammonium bicarbonate, which was repeated twice. After the last the wash, a minimum amount of buffer was left to cover the beads. The cysteines were reduced with 30 µL of 10 mM DTT and alkylated with 30 µL of 55 mM iodoacetamide. Proteins were digested on beads with 1 µg trypsin (Promega, UK) for 18 hours at 37°C. Peptides were acidified with the addition of 4 µL formic acid 2% (v/v). The bead/peptide mix was then centrifuged at 14,000 rcf for 5 minutes and 5 µL of supernatant were diluted with 15 µL of 0.1% formic acid. 5 µL of the diluted supernatant was injected for LC-MS/MS analysis. LC-MS/MS was performed on an Ultimate U3000 HPLC (ThermoFisher Scientific) hyphenated to an Orbitrap QExactive HFX mass spectrometer (ThermoFisher Scientific). Peptides were trapped on a C18 Acclaim PepMap 100 (5 µm, 300 µm x 5mm) trap column (ThermoFisher Scientific) and eluted onto a C18 Acclaim PepMap100 3 µm, 75 µm x 250 mm (ThermoScientific Dionex) using an 85-minute gradient of acetonitrile (5 to 35%). For data dependent acquisition, MS1 scans were acquired at a resolution of 120,000 (AGC target of 3e6 ions with a maximum injection time of 25ms) followed by 25 MS2 scans acquired at a resolution of 30,000 (AGC target of 5e4 ions with a maximum injection time of 150ms) using a collision induced dissociation energy of 27. Dynamic exclusion of fragmented m/z values was set to 50s. Raw data were imported and processed in Proteome Discoverer v3.1 (Thermo Fisher Scientific). The raw files were submitted to a database search using Proteome Discoverer with Sequest HT against the UniProt reference proteome for Homo sapiens. The processing step consisted of a double iterative search using INFERIS Rescoring algorithm on a first pass with methionine oxidation and cysteine carbamidomethylation set as variable and fixed modifications, respectively. For the second pass, all spectra with a confidence filter worse than "high" were researched with Sequest HT including additional common protein variable modifications (Deamidated (N,Q); gln to pyro-Glu (Q); N-terminal acetylation and Methionine loss). The spectra identification was performed with the following

parameters: MS accuracy, 10 p.p.m.; MS/MS accuracy of 0.02 Da; up to two trypsin missed cleavage sites were allowed. Percolator node was used for false discovery rate estimation and only rank 1 peptide identifications of high confidence (FDR<1%) were accepted. Three biological replicates were performed for each sample.

Mitochondria relocation assay

HeLa GFP^{MTS}, GFP-BICD2N^{MTS} or GFP-ScaC^{MTS} cells were treated with 10 µg/mL tetracycline overnight to induce transgene expression. Staining was performed with 20 µM Hoechst (ThermoFisher), 5 µg/mL CellMask Orange (ThermoFisher) and 50 nM MitoTracker Deep Red (ThermoFisher) for 20 minutes at 37˚C. Samples were imaged using a Nikon Ti2 inverted fluorescence microscope with a 20x/0.75NA Air lens. For the mitochondria relocation assay with nocodazole, GFP-ScaC^{MTS} cells were treated with either DMSO or 10 µM nocodazole for 3 hours at 37˚C prior to imaging. For the mitochondrial relocation assay with siRNA knockdowns, GFP^{MTS} and GFP-ScaC^{MTS} cells were transfected with 10 nM of either a non-targeting (scrambled) siRNA (Silencer Select Negative Control #1 siRNA, Invitrogen) or siRNAs directed against *BICD1* (Invitrogen, ID: 147217) or *BICD2* (Invitrogen, ID: 136849) using Lipofectamine RNAiMax (ThermoFisher) according to manufacturer instructions. In some conditions, siRNAs against BICD1 and BICD2 were used in combination, for a final siRNA concentration of 20 nM. Imaging was performed 72 hours after siRNA transfection. Three biological replicates were performed for each sample and condition. Mitochondrial spread relative to the nucleus was quantified using a custom-made ImageJ script (available at https://github.com/jboulanger/imagej-macro/tree/main/Cell_Organization) as previously described[26,52]. The mitochondrial regions, the nucleus and the cell border were defined by segmentation of MitoTracker, Hoechst and CellMask signals, respectively. The mitochondrial spread was measured as the trace of the second moment matrix of the MitoTracker signal intensity in each cell, akin to a standard deviation in 2D.

Immunofluorescence analysis of BICD1 and BICD2

HeLa GFP^{MTS} and GFP-ScaC^{MTS} cells were fixed with 4% PFA in PBS for 10 minutes at room temperature followed by permeabilization with 0.1% Triton X-100 in PBS for 10 minutes at room temperature. Blocking was carried out with 2% BSA in PBS with 0.1% Tween 20 for 1 hour at room temperature. Samples were incubated with anti-BICD1 (Atlas Antibodies, HPA041309, 1:200 dilution) or anti-BICD2 (Atlas Antibodies, HPA023013, 1:200 dilution) antibodies diluted in 1% BSA in PBS solution overnight at 4˚C. Secondary antibody incubation was carried out for 1 hour at room temperature with GFP-Booster Alexa Fluor 488 (Chromotek, gb2AF488, 1:500 dilution) and Alexa Fluor 647 donkey anti-rabbit IgG (ThermoFisher, A-31573, 1:1000 dilution) diluted in 1% BSA in PBS. Samples were mounted using Mounting Medium with DAPI (Abcam, ab104139) and imaged with a Nikon W1 Spinning Disk inverted microscope using a 100x/1.4NA Oil lens. Three biological replicates were performed for each sample. Colocalization of BICD1 and BICD2 with GFP^{MTS} and GFP-ScaC^{MTS} was quantified using a custom-made python script. Cells were segmented using Cellpose [53]. After applying a gaussian filter to the signals for BICD1/2 and GFP^{MTS}/GFP-ScaC^{MTS}, colocalization was quantified based on the Mander's coefficient (M1), which measures the fraction of the total BICD1/2 fluorescent signal that overlaps with fluorescence in the GFP^{MTS}/GFP-ScaC^{MTS} channel.

qPCR analysis of BICD1 and BICD2 expression

Total RNA was extracted from GFP-ScaC^{MTS} cells using the RNeasy RNA extraction kit (Qiagen) according to manufacturer instructions. cDNA was synthesized using the ProtoScript First Stand cDNA Synthesis Kit (NEB). The obtained cDNA was diluted 10-fold to 200 µL with nuclease-free water. qPCR reactions were assembled using 5 µL of Fast SYBR Green Master Mix (ThermoFisher), 1 µL of each primer (final concentration 200 nM), 1 µL of diluted cDNA and nuclease-free water for a final volume of 10 µL. Three biological replicates were performed, each including two technical duplicates. The primers used were: BICD1-F (CTTGTCTTTGTCAGGTAGCC), BICD1-R (CCCATGTCCGCTCAATAAG), BICD2-F (GACGGAGCTGAAGCAGTTG), BICD2-R (CCGGAATTTGTACTCCTTGATGTC), GAPDH-F (TTGGCTACAGCAACAGGGTG) and GAPDH-R (GGGGAGATTCAGTGTGGTGG). For quantification, we used the log2(-ΔCt) method normalizing BICD1 and BICD2 expression to GAPDH expression.

Bacterial propagation and quantitation

The *O. tsutsugamushi* strain UT76 was propagated in HeLa cells and purified as described previously[54]. Purified bacteria were stored at -80 ˚C. For infection of HeLa cells, frozen bacteria were used to infect the cells directly with MOI 50:1.

Immunofluorescence analysis of bacterial localization

HeLa ATCC cells were seeded into sterile µ-Slide 8-well ibiTreat dishes (Ibidi) at a density of $1x10^4$ cells/well and incubated overnight at 37˚C. Cells were transfected with either a scrambled siRNA (Silencer Select Negative Control #1, Invitrogen) or siRNAs targeted against *BICD1* (Invitrogen, ID: 147217) and *BICD2* (Invitrogen, ID: 136849) using Lipofectamine 3000 (Invitrogen) for a final siRNA concentration of 50 nM. After 24 hours, the cells were incubated with *O. tsutsugamushi* at MOI 50:1 for 3 hours, followed by media replacement to remove excess bacteria. At 24 hours post-infection, cells were fixed with 4% formaldehyde for 10 minutes at room temperature. Cells were permeabilized by incubation with absolute ethanol for 1 hour on ice followed by incubation with 0.5% Triton X-100 in PBS for 30 minutes on ice. Permeabilized cells were washed twice with PBS and incubated with an in-house generated antibody against Tsa56 (rat monoclonal, 1:200 dilution) diluted in PBS containing 1mg/ml BSA at 4 °C overnight. Cells were then

washed twice with PBS and incubated with a goat anti-rat Alexa Fluor 488 antibody (ThermoFisher**, A-11006,** 1:1000 dilution), DAPI (1:1000) and HCS CellMask deep red (ThermoFisher, 1:5000 dilution) for 30 min at 37°C in the dark. Cells were maintained in mounting medium (20 mM Tris pH 8.0, 0.5% N-propyl-gallate, 90% glycerol). Imaging was performed using a Zeiss LSM 700 confocal fluorescence microscope with an HBO 100 illuminating system equipped with a 63×/1.4 Plan-APOCHROMAT objective lens (Carl Zeiss) and 405 nm, 488 nm, and 555 nm laser lines acquired ZEN 2011 SP7 FP3 (version 14.0.0.0) software. The distance between *O. tsutsugamushi* and the nucleus was measured using CellProfiler. In brief, the host cell nucleus was segmented using an adaptive strategy (Otsu's method) with adaptive window 24, in which the cytosol was defined as a secondary object correlated with the nucleus. *O. tsutsugamushi* was segmented using a global Otsu's strategy. The distance between cytosolic *O. tsutsugamushi* (i.e. present in the cytosol and non-overlapping with the nucleus) and the nucleus was determined using the "expand until adjacent" method, in which the closet distance between the nuclear rim and the border of the *O. tsutsugamushi* object is measured.

SEC reconstitution assays

For SEC reconstitution experiments, proteins were mixed and incubated on ice for 15 minutes to allow for complex formation. BICD2 and ScaC constructs were mixed in a 1:2 molar ratio. BICD2N and BICD2C were mixed in a 1:1 molar ratio. Complexes were diluted to a final volume of 50 µL in GF150 buffer and injected into a Superose 6 Increase 3.2/300 column pre-equilibrated with GF150 buffer using a 100 µL loop. Fractions underlying protein peaks were visualized by SDS-PAGE followed by Comassie Blue staining.

SEC-MALS

The molecular masses of BICD2, ScaC and the BICD2:ScaC complex were determined in solution using SEC-MALS. Measurements were performed using a Wyatt Heleos II 18 angle light scattering instrument coupled to a Wyatt Optilab rEX online refractive index detector. Samples at a concentration of 1 mg/mL were resolved on a Superose 6 10/300 analytical gel filtration column coupled to an Agilent 1200 series LC system running at 0.5 ml/min in GF150 buffer before then passing through the light scattering and refractive index detectors in a standard SEC MALS format. Protein concentration was determined from the excess differential refractive index based on 0.186 ΔRI for 1 g/ml or with the sequence-based UV extinction coefficient determined in ProtParam. The measured protein concentration and scattering intensity were used to calculate molecular mass from the intercept of a Debye plot using Zimm's model as implemented in Wyatt's ASTRA software. The experimental setup was verified for each set of runs using a BSA standard run of the same sample volume. The BSA monomer peak was used to check mass determination and to evaluate interdetector delay volumes and band broadening parameters that were subsequently applied during analysis of BICD2, ScaC and BICD2:ScaC.

Circular dichroism

Measurements were made in GF150 buffer (25 mM HEPES pH 7.2, 150 mM KCl, 1 mM $MgCl_2$, 1 mM DTT) using a Jasco 815 Spectropolarimeter and a 0.1cm pathlength cuvette. Spectra were recorded at 25°C as the average of 8 scans using 2 mg/ml concentration of ScaC protein with a scan rate of 50 nm/min, bandwidth 1nm and corrected for the contribution of buffer by subtraction of a GF150 blank.

In vitro pulldown assays

For in vitro pull-down of strep-tagged proteins, 200 nM of strep-tagged $BICD2^{711-800}$ (either wild-type or L742A, L786A and L742A/L786A mutant versions) were mixed with 700 nM of either GCN4-$RANBP2^{min}$, $RAB6^{Q72L}$ or ScaC in GF100 buffer (25 mM HEPES pH 7.2, 100 mM KCl, 1mM DTT) and were incubated on ice for 20 minutes to allow for complex formation. Complexes were then diluted to 150 µL with GF100 buffer and 5 µL were set aside for input analysis by SDS-PAGE. Samples were incubated with 30 µL of StrepTactin Sepharose beads (IBA Lifesciences) pre-equilibrated in GF100 for 20 minutes at 4˚C on a rotator (speed 20 rpm). Beads were washed 5 times with 500 µL of GF150 buffer (25 mM HEPES pH 7.2, 150 mM KCl, 1mM DTT). Bound fractions were eluted by incubating the beads with 100 µL GF150 supplemented with 3 mM desthiobiotin for 10 minutes at 4˚C on a rotor (speed 20 rpm). 20 µL of eluate were mixed with 5 µL NuPAGE LDS Sample Buffer (4X) (ThermoFisher), boiled at 95˚C for 10 minutes and loaded onto a SDS-PAGE gel. Bands were visualized by Comassie Blue staining.

Cross-linking mass spectrometry

50 µg of BICD2:ScaC complex were cross-linked for 60 minutes at room temperature at a 1:500 EDC ratio and quenched with 50 mM Tris buffer. The quenched solution was reduced with 5 mM DTT and alkylated with 20 mM idoacetamide. An established SP3 protocol[55,56] was used to clean-up and buffer exchange the reduced and alkylated protein. Briefly, proteins were washed with ethanol using magnetic beads for protein capture and binding. The proteins were resuspended in 100 mM NH_4HCO_3 and digested with trypsin (Promega, UK) at an enzyme-to-substrate ratio of 1:20 and protease max 0.1% (Promega, UK). Digestion was carried out overnight at 37 °C. Clean-up of peptide digests was performed using HyperSep SpinTip P-20 (Thermo Scientific) C18 columns, with 80% Acetonitrile as the elution solvent. Peptides were then evaporated to dryness *via* Speed Vac Plus (Savant, USA). Dried peptides were suspended in 3% Acetonitrile and 0.1 % formic acid and analysed by nano-scale capillary LC-MS/MS using a Ultimate U3000 HPLC (Thermo Scientific) to deliver a flow of approximately 250 nL/min. Peptides were trapped on a C18 Acclaim PepMap100 5 µm, 100 µm x 20 mm nanoViper (Thermo Scientific) before separation on a PepMap RSLC C18, 2 µm, 100 A, 75 µm x 50 cm EasySpray column (Thermo Scientific). Peptides were eluted on a 120-minute gradient with acetonitrile and

interfaced *via* an EasySpray ionisation source to a quadrupole Orbitrap mass spectrometer (Q-Exactive HFX, ThermoScientific, USA). MS data were acquired in data dependent mode with a Top-25 method. High resolution full mass scans were carried out (R = 120,000, *m/z* 400 – 1550) followed by higher energy collision dissociation (HCD) with stepped collision energy range 26, 30, 34 % normalised collision energy. The tandem mass spectra were recorded (R=60,000, AGC target = 1 x 10^5, maximum IT = 120 ms, isolation window *m/z* 1.6, dynamic exclusion 50 s). For analysis of cross-linking data, Xcalibur raw files were converted to MGF files using ProteoWizard[57] and cross-links were analysed by MeroX[58]. Searches were performed against a database containing only BICD2 and ScaC sequences to minimise analysis time with a decoy data base based on peptide sequence shuffling/reversing. Search conditions used 3 maximum missed cleavages with a minimum peptide length of 5, cross-linking targeted residues were K, S, T, and Y, cross-linking modification masses were 54.01056 Da and 85.98264 Da. Variable modifications were carbmidomethylation of cysteine (57.02146 Da) and Methionine oxidation (15.99491 Da). False discovery rate was set to 1 %, and assigned cross-linked spectra were manually inspected.

In vitro TIRF motility assay

Microtubules were made by mixing 4 µg of HiLyte Fluor 488 tubulin (Cytoskeleton), 4 µg of biotinylated tubulin (Cytoskeleton) and 100 µg of unlabelled pig tubulin in BRB80 buffer (80 mM PIPES pH 6.8, 1 mM $MgCl_2$, 1 mM EGTA, 1 mM DTT) for a final volume of 10 µL. 10 µL of polymerization buffer (2X BRB80 buffer, 20% (v/v) DMSO, 2 mM Mg-GTP) were added to the tubulin mix for a total volume of 20 µL. The reaction was incubated on ice for 5 minutes, followed by incubation at 37˚C for 2 hours in the dark. Microtubules were spun at 15,000 rcf for 8 minutes and the supernatant was aspirated to remove non-polymerised tubulin. The microtubule pellet was resuspended in 100 µL Taxol-BRB80 buffer (BRB80 supplemented with 40 µM paclitaxel), followed by another round of centrifugation at 15,000 rcf for 8 minutes. The pellet was resuspended in 60 µL Taxol-BRB80 buffer and microtubule concentration was measured by Bradford assay. Microtubules were diluted to a final concentration of 0.6 mg/mL in Taxol-BRB80 buffer and stored overnight at room temperature in the dark.

The motility chambers were assembled by applying two thin (7-8 mm) strips of double-sided tape (Tesa) on a glass slide, spaced approximately 4-5 mm apart, and attaching on top a coverslip pre-cleaned with piranha solution. The chambers were incubated with PLL-PEG-Biotin (SuSOS AG) to functionalize the coverslip, followed by two washes with 10 µL TIRF buffer (30 mM HEPES pH 7.2, 5 mM MgSO4, 1 mM EGTA, 2 mM DTT) and a wash with 10 µL streptavidin (NEB). The chamber was further washed with 10 µL TIRF buffer followed by a 1-minute incubation with 2 µL of microtubules diluted in 8 µL TIRF buffer supplemented with 50 mM KCl and 1.25 mg/mL casein (TIRF-Casein). Unbound microtubules were washed out with 20 µL TIRF-Casein buffer.

For complex formation, individual proteins were first diluted in TIRF-Casein buffer to the following final concentrations: TMR-dynein to 0.4 mg/mL, dynactin to 0.4 mg/mL, BICD2N to 0.8 mg/mL, BICD2 to 1.2 mg/mL, BICD2-AF488 to 1.5 mg/mL, ScaC to 0.6 mg/mL, ScaC-AF647 to 1.2 mg/mL and Lis1 to 0.4 mg/mL. Complexes were assembled by mixing 1 µL of each diluted protein and incubating on ice for 15 minutes. Complexes were then diluted to a final volume of 10 µL in TIRF-Casein buffer. 1 µL of diluted complex was added to 19 µL of motility reaction buffer (TIRF-Casein Buffer supplemented with 0.2 mg/mL catalase, 1.5 mg/mL glucose oxidase, 0.45% (w/v) glucose, 1% BME and 5 mM Mg-ATP). 10 µL of the motility reaction were flown into the chamber and the sample was imaged immediately using a TIRF microscope (Nikon Eclipse Ti inverted microscope equipped with a Nikon 100x TIRF oil immersion objective). For single-colour samples, an image of the microtubules was taken using the 488 nm laser, and a 500-frame movie (200 ms exposure) was acquired using the 571 nm laser. For dual-colour imaging of ScaC-AF647 and BICD2-488, movies were acquired using the 488 nm and 647 nm lasers. For dual-colour imaging of ScaC-AF647 and TMR-dynein, we used a DV2 beam splitter (Photometrics), which projected each channel onto a different half of the image. Three replicates were performed for each complex combination. For image analysis, kymographs were generated from tiff movie stacks using Fiji. For the quantification of processive events per microtubule µm per minute, processive runs were selected based on previously defined criteria[16]. Velocity was calculated using a pixel size of 105 nm and a frame rate of 236 ms/frame. The fraction of complexes containing both TMR-dynein and ScaC-AF647 was calculated as the number of dual colour events divided by the total number of TMR-dynein events and by the labelling efficiency of ScaC-AF647 (which was determined to be approximately 90.6%).

Immunoblotting analysis and antibodies

For western blot analysis, membranes were blocked with 5% milk in TBST buffer (20 mM Tris, 150 mM NaCl, 0.1% (w/v) Tween 20) for 45 minutes at room temperature. Primary antibody incubation was carried out in 5% milk in TBST for either 2 hours at room temperature or overnight at 4˚C. Secondary antibody incubation was carried out in 5% milk in TBST for 1 hour at room temperature. Chemiluminescent detection was performed using ECL western blot detection reagent (Cytiva). Primary antibodies used were: rabbit polyclonal anti-BICD1 (Atlas Antibodies HPA041309, 1:1000 dilution), rabbit polyclonal anti-BICD2 (Atlas Antibodies HPA023013, 1:1000 dilution), mouse monoclonal anti-GAPDH (Abcam, ab8245, 1:1000 dilution), mouse monoclonal anti-β-tubulin (Sigma, T4026). Secondary antibodies used were: goat anti-rabbit IgG HRP (Abcam, ab6721, 1:2000 dilution) and goat anti-mouse IgG HRP (Dako, P0447, 1:1500 dilution).

AlphaFold prediction

Structure predictions were performed using Alphafold2 or Alphafold2-Multimer through a local installation of ColabFold. The structures of ScaC (UniProt I6Z768) residues 33-223 and BICD2 (UniProt Q921C5) residues 711-800 were predicted by running ColabFold 1.3.0 on two copies of these segments. The interactions between BICD2 (residues 650-800) and Rab6 (UniProt P20340) or RanBP2 (UniProt P49792) residues 2148-2240 were predicted by running ColabFold 1.3.0 on two copies of BICD2 and one copy of either Rab6 or RanBP2.

Statistical analysis

Statistical analysis was performed in R. Details on the specific statistical test used for each experiment can be found in the respective figure legend. Plots were made using R.

Data availability

AlphaFold structure models have been deposited on ModelArchive (modelarchive.org) and are available with the accession codes ma-0p39h (BICD2 residues 711-800), ma-amwrh (ScaC residues 33-223), ma-2nlcr (BICD2 residues 650-800 in complex with RAB6A) and ma-hss3s (BICD2 residues 650-800 in complex with RANBP2 residues 2148-2240). Light microscopy data, proteomics data, western blots and SDS-PAGE gels are available at 10.5281/zenodo.10845305.

Acknowledgments

We thank C.M. Johnson for assistance and analysis of SEC-MALS and CD experiments. We thank F. Begum and C. Franco for providing support with mass spectrometry experiments and data analysis. We thank M. Laub for assistance with Python image analysis. We thank S. Bullock and Y. Andres Jeske for help with the HeLa Flp-In T-REX FRT-TO system. We thank K. Singh and C.K. Lau for help with protein purification. We thank F. Randow for helpful discussion. This work was supported by a Boehringer Ingelheim Fonds PhD Fellowship to G.M., a Wellcome Investigator Award to A.P.C. (210711/Z/18/Z and 227434/Z/23/Z), a Wellcome Trust Senior Research Fellowship to J.S. (224277/Z/21/Z) and Medical Research Council funding to A.P.C. (MC_UP_A025_1011).

Author contributions

G.M. performed cloning, protein purification, biochemical assays, single molecule assays, cellular experiments and data analysis. K.S. and C.K. performed infection experiments and data analysis. J.B. performed image analysis. T.E.M., H.K. and G.M. performed cross-linking mass spectrometry. J.S., A.P.C. and G.M. conceived the project. G.M. wrote the manuscript with input from all authors.

Competing interest

The authors declare no competing interests.

REFERENCES

1. Haglund, C.M. & Welch, M.D. Pathogens and polymers: microbe-host interactions illuminate the cytoskeleton. *J Cell Biol* **195**, 7-17 (2011).
2. Kim, S.W. et al. Microtubule- and dynein-mediated movement of Orientia tsutsugamushi to the microtubule organizing center. *Infect Immun* **69**, 494-500 (2001).
3. Clausen, J.D., Christiansen, G., Holst, H.U. & Birkelund, S. Chlamydia trachomatis utilizes the host cell microtubule network during early events of infection. *Mol Microbiol* **25**, 441-9 (1997).
4. Grieshaber, S.S., Grieshaber, N.A. & Hackstadt, T. Chlamydia trachomatis uses host cell dynein to traffic to the microtubule-organizing center in a p50 dynamitin-independent process. *J Cell Sci* **116**, 3793-802 (2003).
5. Salje, J. Orientia tsutsugamushi: A neglected but fascinating obligate intracellular bacterial pathogen. *PLoS Pathog* **13**, e1006657 (2017).
6. Luce-Fedrow, A. et al. A Review of Scrub Typhus (Orientia tsutsugamushi and Related Organisms): Then, Now, and Tomorrow. *Trop Med Infect Dis* **3**(2018).
7. Seong, S.Y., Choi, M.S. & Kim, I.S. Orientia tsutsugamushi infection: overview and immune responses. *Microbes Infect* **3**, 11-21 (2001).
8. Ge, Y. & Rikihisa, Y. Subversion of host cell signaling by Orientia tsutsugamushi. *Microbes Infect* **13**, 638-48 (2011).
9. Paris, D.H. et al. Orientia tsutsugamushi in human scrub typhus eschars shows tropism for dendritic cells and monocytes rather than endothelium. *PLoS Negl Trop Dis* **6**, e1466 (2012).
10. Moron, C.G., Popov, V.L., Feng, H.M., Wear, D. & Walker, D.H. Identification of the target cells of Orientia tsutsugamushi in human cases of scrub typhus. *Mod Pathol* **14**, 752-9 (2001).
11. Atwal, S. et al. The obligate intracellular bacterium Orientia tsutsugamushi differentiates into a developmentally distinct extracellular state. *Nat Commun* **13**, 3603 (2022).
12. Chu, H. et al. Exploitation of the endocytic pathway by Orientia tsutsugamushi in nonprofessional phagocytes. *Infect Immun* **74**, 4246-53 (2006).
13. Kim, M.J., Kim, M.K. & Kang, J.S. Involvement of lipid rafts in the budding-like exit of Orientia tsutsugamushi. *Microb Pathog* **63**, 37-43 (2013).
14. Rikihisa, Y. & Ito, S. Localization of electron-dense tracers during entry of Rickettsia tsutsugamushi into polymorphonuclear leukocytes. *Infect Immun* **30**, 231-43 (1980).
15. Reck-Peterson, S.L., Redwine, W.B., Vale, R.D. & Carter, A.P. The cytoplasmic dynein transport machinery and its many cargoes. *Nat Rev Mol Cell Biol* **19**, 382-398 (2018).
16. Schlager, M.A., Hoang, H.T., Urnavicius, L., Bullock, S.L. & Carter, A.P. In vitro reconstitution of a highly processive recombinant human dynein complex. *EMBO J* **33**, 1855-68 (2014).
17. McKenney, R.J., Huynh, W., Tanenbaum, M.E., Bhabha, G. & Vale, R.D. Activation of

cytoplasmic dynein motility by dynactin-cargo adapter complexes. *Science* **345**, 337-41 (2014).
18. Olenick, M.A. & Holzbaur, E.L.F. Dynein activators and adaptors at a glance. *J Cell Sci* **132**(2019).
19. Ha, N.Y., Cho, N.H., Kim, Y.S., Choi, M.S. & Kim, I.S. An autotransporter protein from Orientia tsutsugamushi mediates adherence to nonphagocytic host cells. *Infect Immun* **79**, 1718-27 (2011).
20. Ha, N.Y. et al. Detection of antibodies against Orientia tsutsugamushi Sca proteins in scrub typhus patients and genetic variation of sca genes of different strains. *Clin Vaccine Immunol* **19**, 1442-51 (2012).
21. Koralur, M.C., Ramaiah, A. & Dasch, G.A. Detection and distribution of Sca autotransporter protein antigens in diverse isolates of Orientia tsutsugamushi. *PLoS Negl Trop Dis* **12**, e0006784 (2018).
22. Haglund, C.M., Choe, J.E., Skau, C.T., Kovar, D.R. & Welch, M.D. Rickettsia Sca2 is a bacterial formin-like mediator of actin-based motility. *Nat Cell Biol* **12**, 1057-63 (2010).
23. Kleba, B., Clark, T.R., Lutter, E.I., Ellison, D.W. & Hackstadt, T. Disruption of the Rickettsia rickettsii Sca2 autotransporter inhibits actin-based motility. *Infect Immun* **78**, 2240-7 (2010).
24. Hoogenraad, C.C. et al. Mammalian Golgi-associated Bicaudal-D2 functions in the dynein-dynactin pathway by interacting with these complexes. *EMBO J* **20**, 4041-54 (2001).
25. Hoogenraad, C.C. et al. Bicaudal D induces selective dynein-mediated microtubule minus end-directed transport. *EMBO J* **22**, 6004-15 (2003).
26. Singh, K. et al. Molecular mechanism of dynein-dynactin complex assembly by LIS1. *Science* **383**, eadk8544 (2024).
27. Olenick, M.A., Tokito, M., Boczkowska, M., Dominguez, R. & Holzbaur, E.L. Hook Adaptors Induce Unidirectional Processive Motility by Enhancing the Dynein-Dynactin Interaction. *J Biol Chem* **291**, 18239-51 (2016).
28. Wong, C.H. et al. Genome-scale requirements for dynein-based transport revealed by a high-content arrayed CRISPR screen. *J Cell Biol* **223**(2024).
29. Liu, Y. et al. Bicaudal-D uses a parallel, homodimeric coiled coil with heterotypic registry to coordinate recruitment of cargos to dynein. *Genes Dev* **27**, 1233-46 (2013).
30. Splinter, D. et al. Bicaudal D2, dynein, and kinesin-1 associate with nuclear pore complexes and regulate centrosome and nuclear positioning during mitotic entry. *PLoS Biol* **8**, e1000350 (2010).
31. Matanis, T. et al. Bicaudal-D regulates COPI-independent Golgi-ER transport by recruiting the dynein-dynactin motor complex. *Nat Cell Biol* **4**, 986-92 (2002).
32. Short, B., Preisinger, C., Schaletzky, J., Kopajtich, R. & Barr, F.A. The Rab6 GTPase regulates recruitment of the dynactin complex to Golgi membranes. *Curr Biol* **12**, 1792-5 (2002).
33. Terawaki, S., Yoshikane, A., Higuchi, Y. & Wakamatsu, K. Structural basis for cargo binding and autoinhibition of Bicaudal-D1 by a parallel coiled-coil with homotypic registry. *Biochem Biophys Res Commun* **460**, 451-6 (2015).
34. Cui, H. et al. Adapter Proteins for Opposing Motors Interact Simultaneously with Nuclear Pore Protein Nup358. *Biochemistry* **58**, 5085-5097 (2019).
35. Noell, C.R. et al. A Quantitative Model for BicD2/Cargo Interactions. *Biochemistry* **57**, 6538-6550 (2018).
36. Schlager, M.A. et al. Pericentrosomal targeting of Rab6 secretory vesicles by Bicaudal-D-related protein 1 (BICDR-1) regulates neuritogenesis. *EMBO J* **29**, 1637-51 (2010).
37. Sladewski, T.E. et al. Recruitment of two dyneins to an mRNA-dependent Bicaudal D transport complex. *Elife* **7**(2018).
38. Huynh, W. & Vale, R.D. Disease-associated mutations in human BICD2 hyperactivate motility of dynein-dynactin. *J Cell Biol* **216**, 3051-3060 (2017).
39. Gibson, J.M. et al. Coil-to-alpha-helix transition at the Nup358-BicD2 interface activates BicD2 for dynein recruitment. *Elife* **11**(2022).
40. Gouin, E. et al. The RickA protein of Rickettsia conorii activates the Arp2/3 complex. *Nature* **427**, 457-61 (2004).
41. Jeng, R.L. et al. A Rickettsia WASP-like protein activates the Arp2/3 complex and mediates actin-based motility. *Cell Microbiol* **6**, 761-9 (2004).
42. Yoshikawa, Y. et al. Listeria monocytogenes ActA-mediated escape from autophagic recognition. *Nat Cell Biol* **11**, 1233-40 (2009).
43. Meyer, D.H., Rose, J.E., Lippmann, J.E. & Fives-Taylor, P.M. Microtubules are associated with intracellular movement and spread of the periodontopathogen Actinobacillus actinomycetemcomitans. *Infect Immun* **67**, 6518-25 (1999).
44. Hackstadt, T., Rockey, D.D., Heinzen, R.A. & Scidmore, M.A. Chlamydia trachomatis interrupts an exocytic pathway to acquire endogenously synthesized sphingomyelin in transit from the Golgi apparatus to the plasma membrane. *EMBO J* **15**, 964-77 (1996).
45. Thurston, T.L., Wandel, M.P., von Muhlinen, N., Foeglein, A. & Randow, F. Galectin 8 targets damaged vesicles for autophagy to defend cells against bacterial invasion. *Nature* **482**, 414-8 (2012).
46. Uhlen, M. et al. Proteomics. Tissue-based map of the human proteome. *Science* **347**, 1260419 (2015).
47. Dharan, A. et al. Bicaudal D2 facilitates the cytoplasmic trafficking and nuclear import of HIV-1 genomes during infection. *Proc Natl Acad Sci U S A* **114**, E10707-E10716 (2017).
48. Musarrat, F., Chouljenko, V. & Kousoulas, K.G. Cellular and Viral Determinants of HSV-1 Entry and Intracellular Transport towards Nucleus of Infected Cells. *J Virol* (2021).
49. Carnes, S.K., Zhou, J. & Aiken, C. HIV-1 Engages a Dynein-Dynactin-BICD2 Complex for

Infection and Transport to the Nucleus. *J Virol* **92**(2018).
50. Badieyan, S. et al. HIV-1 binds dynein directly to hijack microtubule transport machinery. (BioRxiv [Preprint], 2023).
51. McClintock, M.A. et al. RNA-directed activation of cytoplasmic dynein-1 in reconstituted transport RNPs. *Elife* **7**(2018).
52. Madan, V. et al. HEATR5B associates with dynein-dynactin and promotes motility of AP1-bound endosomal membranes. *EMBO J* **42**, e114473 (2023).
53. Stringer, C., Wang, T., Michaelos, M. & Pachitariu, M. Cellpose: a generalist algorithm for cellular segmentation. *Nat Methods* **18**, 100-106 (2021).
54. Giengkam, S. et al. Improved Quantification, Propagation, Purification and Storage of the Obligate Intracellular Human Pathogen Orientia tsutsugamushi. *PLoS Negl Trop Dis* **9**, e0004009 (2015).
55. Hughes, C.S. et al. Single-pot, solid-phase-enhanced sample preparation for proteomics experiments. *Nat Protoc* **14**, 68-85 (2019).
56. Batth, T.S. et al. Protein Aggregation Capture on Microparticles Enables Multipurpose Proteomics Sample Preparation. *Mol Cell Proteomics* **18**, 1027-1035 (2019).
57. Chambers, M.C. et al. A cross-platform toolkit for mass spectrometry and proteomics. *Nat Biotechnol* **30**, 918-20 (2012).
58. Gotze, M. et al. Automated assignment of MS/MS cleavable cross-links in protein 3D-structure analysis. *J Am Soc Mass Spectrom* **26**, 83-97 (2015).

SUPPLEMENTARY INFORMATION

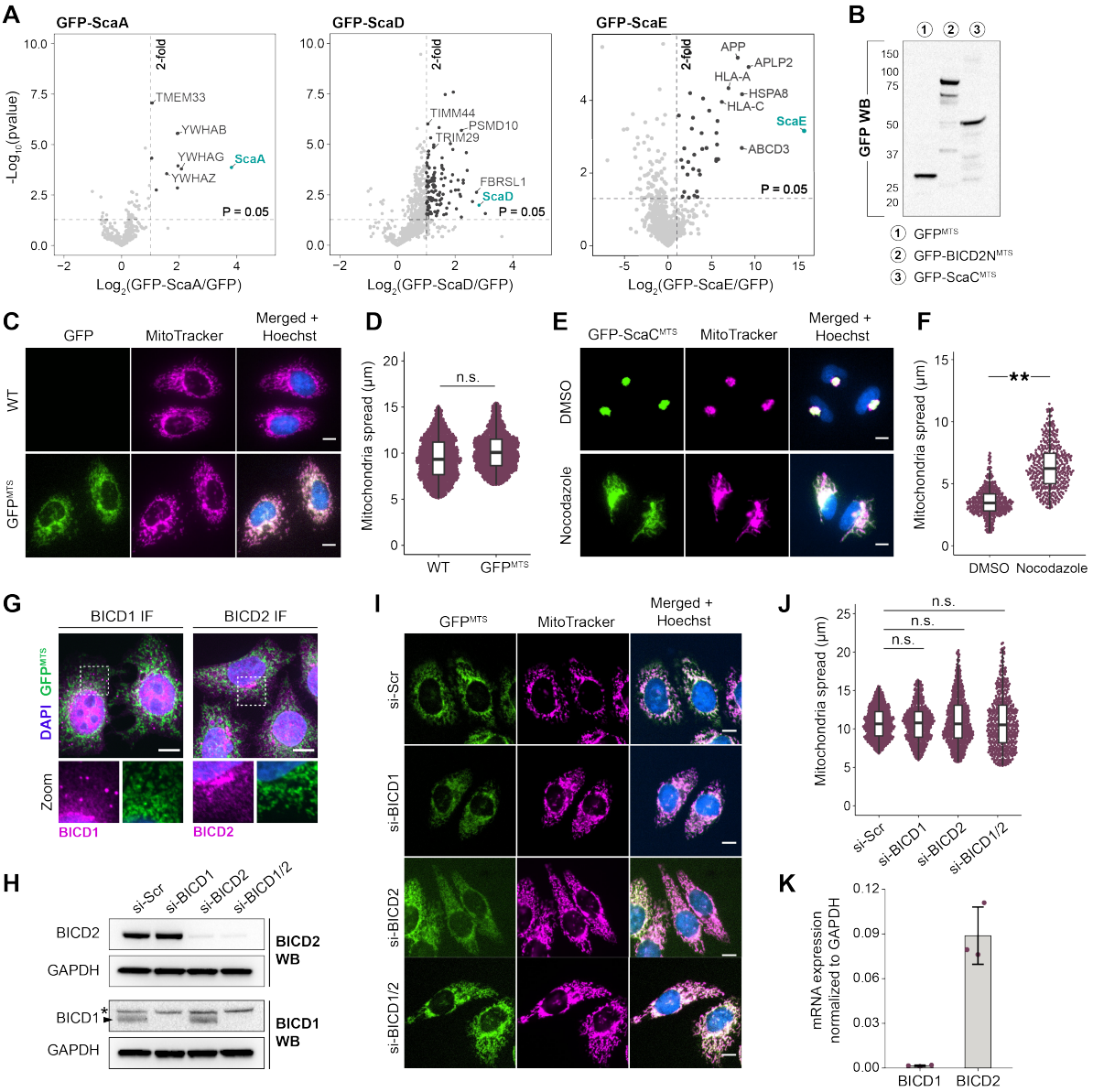

Supplementary Figure 1. The bacterial protein ScaC recruits the activating adaptors BICD1 and BICD2. (A) Volcano plot summarising the results of GFP-ScaA, GFP-ScaD and GFP-ScaE co-IP/MS in HeLa Flp-In cells. The significant enrichment levels were calculated from n=3 independent replicates. Selected hits are indicated. **(B)** Western blot showing expression of GFP^{MTS}, GFP-BICD2N^{MTS} and GFP-ScaC^{MTS} in Hela Flp-In cells. **(C)** Representative images of mitochondrial relocation assay with wild-type and GFP^{MTS} cell lines. Scale bars indicate 10 µm. The corresponding quantification of mitochondria spread is shown in **(D).** P-values were calculated from n=3 independent replicates using a two-tailed T-test. **(E)** Representative images of GFP-ScaC^{MTS} cells treated with either DMSO or 10 µm nocodazole for 3 hours. The corresponding quantification of mitochondria spread is shown in **(F).** P-values were calculated from n=3 independent replicates using a two-tailed T-test. **=p<0.01. **(G)** Representative IF images showing colocalization of GFP^{MTS} with BICD1 and BICD2 respectively. Scale bars indicate 10 µm. **(H)** Western blots showing knockdown of BICD1 and BICD2 upon siRNA treatment. GAPDH was used as a loading control. The asterisk indicates a non-specific GAPDH band. **(I)** Representative images of GFP^{MTS} cells treated with siRNA against BICD1 and/or BICD2. A scrambled siRNA (si-Scr) was used as a negative control. Scale bars indicate 10 µm. **(J)** Quantification of mitochondrial spread in siRNA-treated GFP^{MTS} cells. P-values were calculated from n=3 independent replicates using two-tailed ANOVA (F value = 0.805) and a Tukey HSD post-hoc test. **(K)** Barplot showing mRNA expression of BICD1 and BICD2 relative to GAPDH in HeLa Flp-In GFP-ScaC^{MTS} cells. Error bars indicate mean ± standard deviation.

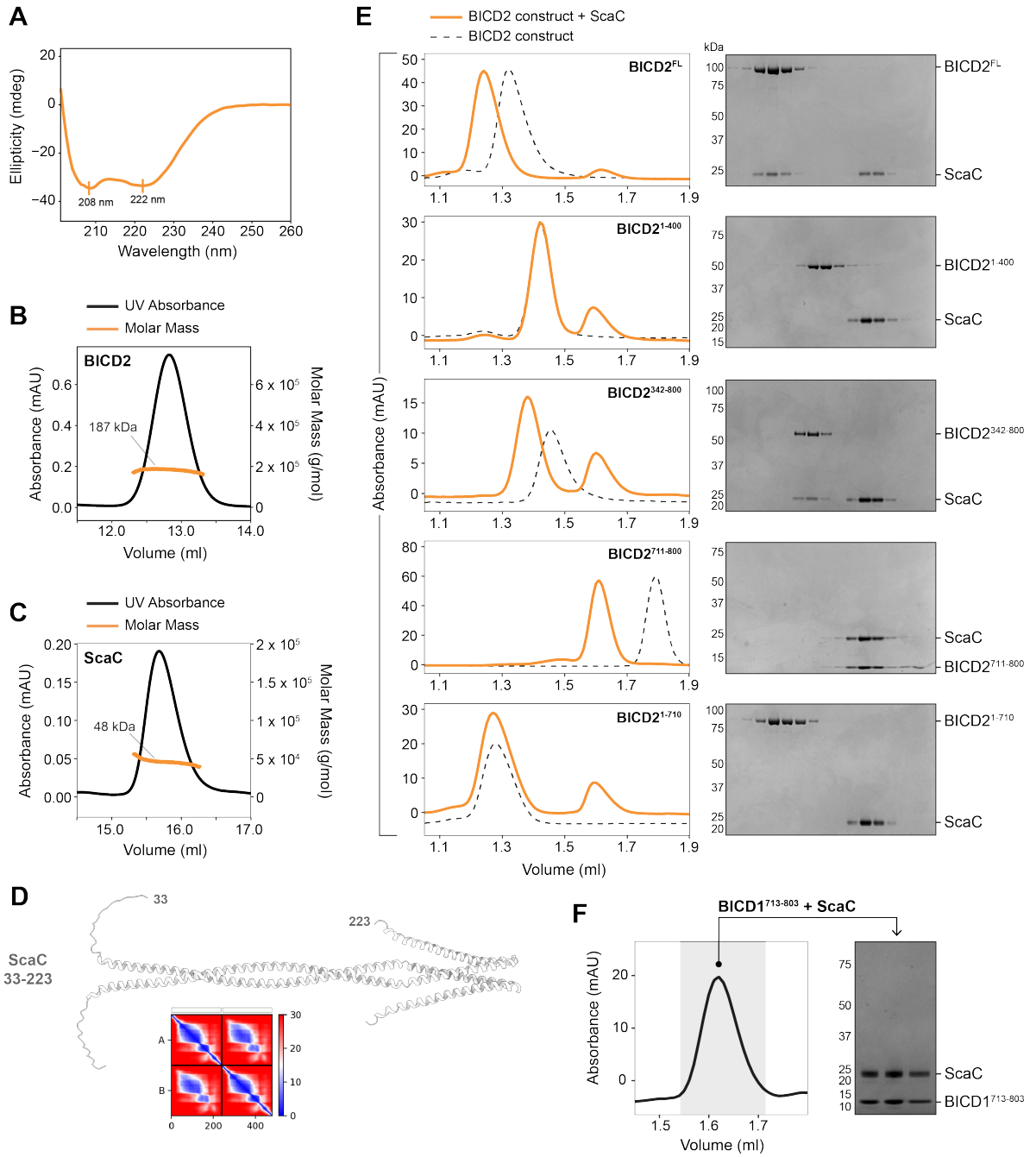

Supplementary Figure 2. ScaC binds the C-terminal CC3 domain of BICD2. (A) Circular dichroism of purified ScaC. 208 nm and 222 nm peaks are indicated. **(B-C)** SEC-MALS of purified BICD2 and ScaC respectively. Molecular masses are indicated for both proteins. The expected monomer molecular weight is 98 kDa for BICD2 and 24 kDa for ScaC. **(D)** Alphafold prediction of the passenger domain of ScaC (residues 33-223). The PAE plot for the prediction is shown. **(E)** Chromatograms showing ScaC in complex with different BICD2 truncations. Dotted lines represent chromatographs of each BICD2 construct in the absence of ScaC. SDS-PAGE gels show fractions underlying the relevant protein peaks. **(F)** Chromatogram showing BICD1$^{713-803}$ in complex with ScaC. SDS-PAGE gels show fractions underlying the relevant protein peaks.

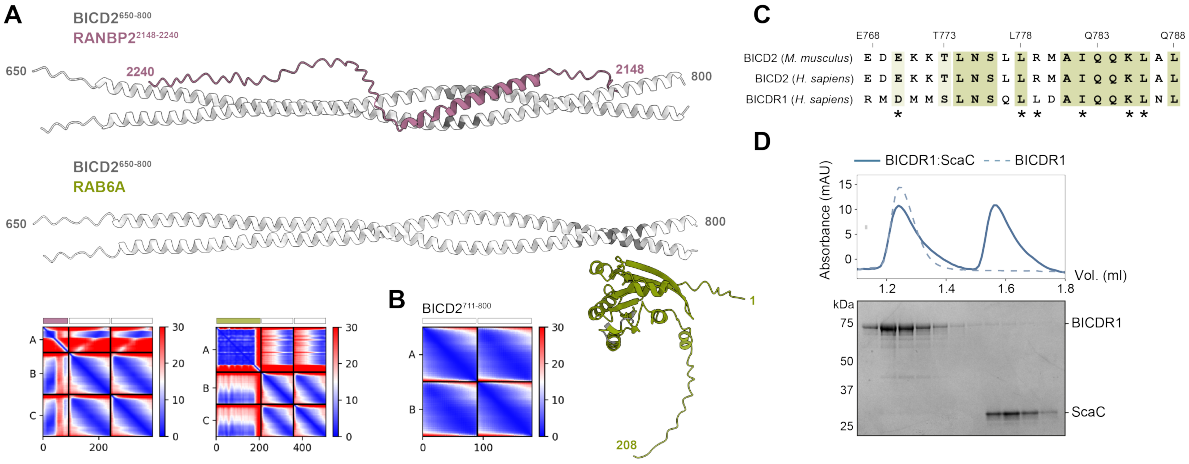

Supplementary Figure 3. ScaC binds BICD2 through a novel interface. (A) AlphaFold predictions of BICD2$^{650-800}$ in complex with either RANBP2$^{2148-2240}$ (top) or RAB6A (bottom). Biochemically validated interface residues are highlighted in grey. PAE plots are shown. **(B)** PAE plot for the AlphaFold prediction of BICD2$^{711-800}$ shown in Figure 3F. **(C)** Multiple sequence alignment of the Rab6-binding site across mouse BICD2, human BICD2 and human BICDR1. Residues numbers refer to murine BICD2. Asterisks indicate residues required for the interaction with Rab6. **(D)** Chromatogram showing BICDR1 in the presence (solid line) or absence (dotted line) of ScaC. SDS-PAGE gels show fractions underlying the relevant protein peaks.

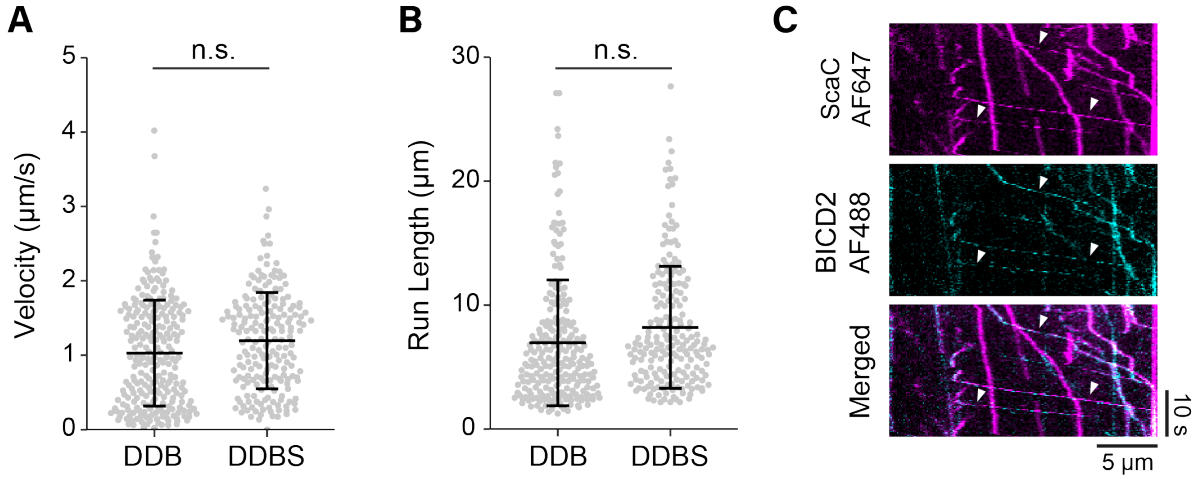

Supplementary Figure 4. ScaC activates BICD2 for dynein motility. (A) Quasi-random scatter plot showing velocity of DDB and DDBS complexes. P-values were calculated from n=3 independent replicates using a two-tailed T- test. **(B)** Quasi-random scatter plot showing run length of DDB and DDBS complexes. P-values were calculated from n=3 independent replicates using a two-tailed T- test. **(C)** Representative kymographs showing colocalization of Scac-AF674 (magenta) and BICD2-AF488 (cyan). Arrows indicate colocalization events. Scale bars are shown.

Supplementary Table 1. Mass spectrometry hits for GFP-ScaA co-IP. List of proteins specifically co-precipitating with GFP-ScaA. MW = molecular weight, FC = $\log_2$(Fold Change), P-Value = $-\log_{10}$(p-value). P-values were calculated from triplicate runs.

UNIPROT ID	GENE NAME	MW (kDa)	P-VALUE	FC
Q04917	YWHAH	28	3.79	2.07
P61981	YWHAG	28	3.95	1.96
P31946	YWHAB	28	5.56	1.95
P27348	YWHAQ	27	2.85	1.94
P62258	YWHAE	29	5.55	1.94
Q9C0I4	THSD7B	179.1	0.86	1.61
P63104	YWHAZ	27	3.56	1.57
P17655	CAPN2	80	2.75	1.21
P57088	TMEM33	28	7.06	1.06
P62910	RPL32	16	4.32	1.05

Supplementary Table 2. Mass spectrometry hits for GFP-ScaD co-IP. List of proteins specifically co-precipitating with GFP-ScaD. MW = molecular weight, FC = log_2(Fold Change), P-Value = -log_{10}(p-value). P-values were calculated from triplicate runs.

UNIPROT ID	GENE NAME	MW (kDa)	P-VALUE	FC
Q04695	KRT17	48	1.57	3.05
Q9HCM7	FBRSL1	111	2.63	2.74
Q01130	SRSF2	26	2.17	2.60
P60660	MYL6	17	3.71	2.42
Q15149	PLEC	532	4.59	2.39
O14950	MYL12B	20	3.22	2.28
P35579	MYH9	226	3.08	2.28
O75832	PSMD10	24	5.70	2.22
P15085	CPA1	47	1.40	2.22
P31153	MAT2A	44	2.42	2.19
Q8WWI1	LMO7	193	2.52	2.17
P42166	TMPO	75	2.74	2.12
Q9ULV4	CORO1C	53	3.23	2.10
P02545	LMNA	74	1.81	2.05
P62280	RPS11	18	2.74	2.01
Q7Z406	MYH14	228	7.59	1.94
P08729	KRT7	51	4.75	1.92
P05783	KRT18	48	3.50	1.91
P42677	RPS27	10	2.67	1.86
P05787	KRT8	54	3.16	1.86
P35580	MYH10	229	5.03	1.84
Q9UHB6	LIMA1	85	2.09	1.79
P62910	RPL32	16	1.84	1.71
P67936	TPM4	29	1.55	1.69
P50402	EMD	29	7.47	1.66
P06753	TPM3	33	3.34	1.65
P62266	RPS23	16	1.51	1.61
P26599	PTBP1	57	2.96	1.60
P08174	CD55	41	3.76	1.59
P07951	TPM2	33	2.52	1.58
Q9UPQ0	LIMCH1	122	4.33	1.55
P62244	RPS15A	15	3.83	1.55
Q15233	NONO	54	3.96	1.54
Q6KB66	KRT80	51	3.55	1.54
P58107	EPPK1	555	2.31	1.54
P15924	DSP	332	3.29	1.52
Q9BUF5	TUBB6	50	2.05	1.51
P08670	VIM	54	2.23	1.48
P09382	LGALS1	15	2.62	1.47

P46777	RPL5	34	2.01	1.47
O95816	BAG2	24	2.48	1.45
O75083	WDR1	66	5.83	1.45
A6NHL2	TUBAL3	50	1.70	1.40
Q14257	RCN2	37	2.50	1.40
O00159	MYO1C	122	1.59	1.37
Q5H8A4	PIGG	108	2.02	1.37
Q9BQE3	TUBA1C	50	1.46	1.35
Q16643	DBN1	71	2.22	1.34
Q08380	LGALS3BP	65	2.71	1.32
Q9Y608	LRRFIP2	82	2.92	1.31
P09874	PARP1	113	1.67	1.30
Q15293	RCN1	39	3.61	1.29
P32969	RPL9; RPL9P7; RPL9P8; RPL9P9	22	2.24	1.29
P20042	EIF2S2	38	3.33	1.29
Q12965	MYO1E	127	3.83	1.29
P17844	DDX5	69	3.18	1.28
P05198	EIF2S1	36	2.99	1.27
P78527	PRKDC	469	2.87	1.27
P62879	GNB2	37	3.50	1.26
Q9Y4I1	MYO5A	215	4.97	1.26
Q14134	TRIM29	66	4.85	1.26
P61513	RPL37A	10	2.63	1.25
Q6ZRV2	FAM83H	127	3.37	1.25
P09012	SNRPA	31	3.18	1.24
P0CG38	POTEI	121	2.99	1.23
Q14498	RBM39	59	2.32	1.22
P35637	FUS	53	3.33	1.20
P57088	TMEM33	28	3.19	1.19
Q9Y5L4	TIMM13	11	2.68	1.19
O15027	SEC16A	252	2.20	1.19
Q14152	EIF3A	167	1.56	1.18
Q9BR76	CORO1B	54	1.57	1.17
P13646	KRT13	50	1.58	1.16
O43795	MYO1B	132	2.37	1.16
P83881	RPL36A	12	3.16	1.16
Q15645	TRIP13	49	5.33	1.15
Q13283	G3BP1	52	1.65	1.15
P14373	TRIM27	59	3.20	1.13
P08754	GNAI3	41	2.33	1.13
P60866	RPS20	13	2.28	1.12
Q9NZI8	IGF2BP1	63	2.32	1.12
Q92974	ARHGEF2	112	1.87	1.11

Q71U36	TUBA1A	50	3.85	1.10
Q12906	ILF3	95	3.82	1.10
O75534	CSDE1	89	1.96	1.09
P62829	RPL23	15	4.49	1.09
Q9ULX6	AKAP8L	72	1.87	1.08
P39748	FEN1	43	2.63	1.08
P49207	RPL34	13	4.66	1.08
Q96EY1	DNAJA3	53	1.54	1.08
Q5T0W9	FAM83B	115	2.38	1.08
Q13045	FLII	145	1.56	1.08
P11142	HSPA8	71	2.92	1.08
Q07666	KHDRBS1	48	3.10	1.08
P46779	RPL28	16	3.40	1.07
Q92841	DDX17	80	1.91	1.06
P61619	SEC61A1	52	3.07	1.06
Q9Y3U8	RPL36	12	1.75	1.06
P07355	ANXA2	39	1.37	1.06
O43615	TIMM44	51	6.02	1.06
P17931	LGALS3	26	4.34	1.06
Q9BZK7	TBL1XR1	56	1.40	1.05
P52272	HNRNPM	78	2.14	1.04
Q13885	TUBB2A	50	1.41	1.04
P62906	RPL10A	25	3.95	1.04
Q15003	NCAPH	83	1.36	1.03
P0CW18	PRSS56	65	2.85	1.03
P61313	RPL15	24	3.19	1.03
P14866	HNRNPL	64	4.08	1.02
O43852	CALU	37	1.55	1.02
P07947	YES1	61	1.36	1.01
Q96AG4	LRRC59	35	3.59	1.01
P27708	CAD	243	2.21	1.01
Q8NE71	ABCF1	96	2.91	1.01
P62917	RPL8	28	2.62	1.01
P49458	SRP9	10	2.08	1.01
P62081	RPS7	22	3.05	1.00
Q7Z2W4	ZC3HAV1	101	1.84	1.00

Supplementary Table 3. Mass spectrometry hits for GFP-ScaE co-IP. List of proteins specifically co-precipitating with GFP-ScaE. MW = molecular weight, FC = $\log_2$(Fold Change), P-Value = $-\log_{10}$(p-value). P-values were calculated from triplicate runs.

UNIPROT ID	GENE NAME	MW (kDa)	P-VALUE	FC
Q06481	APLP2	87	4.91	9.28
E9PK54	HSPA8	20	4.16	8.53
P28288	ABCD3	75	2.69	8.48
E9PG40	APP	81	5.17	8.04
Q53Z42	HLA-A	41	4.33	6.96
Q5QT33	HLA-C;HLA-Cw	42	3.95	6.18
H0YJT4	SAV1	11	2.38	5.78
Q5SPM2	HLA-A	34	3.43	5.70
P78347	GTF2I	112	2.78	5.64
P10124	SRGN	18	3.10	5.57
Q5VZU9	TPP2	130	2.38	5.56
P55084	HADHB	50	2.33	5.55
Q9BZF1	OSBPL8	101	3.71	4.74
Q9H252	KCNH6	106	2.69	4.43
P0DMV9	HSPA1B;HSPA1A	70	4.05	4.04
Q03167	TGFBR3	93	2.66	3.95
Q04721	NOTCH2	265	3.10	3.87
P18031	PTPN1	41	1.96	3.68
Q12933	TRAF2	56	2.07	3.56
J3KR73	RAB6B;RAB6A;RAB39A	6	1.34	3.39
P62917	RPL8	18	1.49	3.32
P61313	RPL15	20	1.38	3.04
H0Y8K0	HSPA9	72	2.50	3.03
Q8NBU5	ATAD1	41	2.11	2.91
P11142	HSPA8	71	3.52	2.88
O95672	ECEL1	88	3.22	2.75
P11021	HSPA5	72	4.19	2.56
Q8TEM1	NUP210	205	5.30	2.53
P46777	RPL5	34	1.33	2.41
P13747	HLA-E	40	2.30	2.34
G3XAI2	LAMB1	183	1.96	2.25
H0YFD6	HADHA	86	2.68	1.88
P00390	GSR	56	1.48	1.88
O14763	TNFRSF10B	48	2.15	1.70
Q00610	CLTC	192	1.35	1.68
Q9UKJ3	GPATCH8	164	2.36	1.54
H0YDX6	CD44	20	3.58	1.26

Supplementary Table 4. Mass spectrometry hits for GFP-ScaC co-IP. List of proteins specifically co-precipitating with GFP-ScaC. BICD1 and BICD2 are highlighted. MW = molecular weight, FC = log_2(Fold Change), P-Value = $-log_{10}$(p-value). P-values were calculated from triplicate runs.

UNIPROT ID	GENE NAME	MW (kDa)	P-VALUE	FC
O00411	POLRMT	139	3.05	11.86
P46063	RECQL	73	5.40	11.39
Q8TD16	**BICD2**	**94**	**4.06**	**10.24**
E9PK54	HSPA8	20	4.16	8.93
Q2M3G4	SHROOM1	91	3.35	8.16
P37198	NUP62	53	3.29	7.34
Q1MSJ5	CSPP1	146	4.05	7.00
Q96CP6	GRAMD1A	90	3.71	6.58
O75665;	OFD1	117	3.35	6.29
Q96G01	**BICD1**	**95**	**3.45**	**6.28**
P08670	VIM	54	2.10	6.13
P41208	CETN2	20	2.73	5.56
Q9GZM8	NDEL1;NDE1	38	3.02	5.08
Q86X02	CDR2L	53	2.86	5.00
Q3KR37	GRAMD1B	81	2.43	4.92
Q6ZRV2	FAM83H	127	3.20	4.84
P14373	TRIM27	58	2.11	4.61
E9PMS6	LMO7	145	3.00	4.16
E9PJP2	SOGA3	103	2.88	4.03
O95816	BAG2	24	3.78	3.89
Q13573	SNW1	65	2.25	3.72
P0DMV9	HSPA1B;HSPA1A	70	3.82	3.59
Q14134	TRIM29	66	2.04	3.58
P11142	HSPA8	71	3.81	3.56
Q5HY57	EMD	29	1.98	3.45
Q96HH9	GRAMD3	48	2.17	3.39
A0A087WTS8	HSPA4	53	2.55	3.37
E5RGQ4	PCM1	210	2.04	3.35
Q14258	TRIM25	71	2.13	3.32
Q8TDB6	DTX3L	84	1.47	3.24
O95817	BAG3	62	1.64	3.11
P50991	CCT4	58	1.92	3.04
Q13751	LAMB3	130	2.50	2.89
Q9NZL4	HSPBP1	39	1.81	2.79
Q15438	CYTH2;CYTH1;CYTH3	47	2.94	2.68
Q9Y3C6	PPIL1	18	1.61	2.55
Q13185	CBX1;CBX3	16	2.36	2.52
Q9BWM7	SFXN3	36	1.49	2.35
E9PIQ7	HAX1	17	1.35	2.26

P31689	DNAJA1	45	2.24	2.00
P11021	HSPA5	72	4.13	1.99
Q01850	CDR2	52	4.33	1.98
D6RCD7	HSPA9	72	1.80	1.90
O94927	HAUS5	72	1.59	1.87
Q8IXQ6	PARP9	96	1.60	1.81
P33993	MCM7	81	1.41	1.67
F5H3X6	PHB2	24	1.44	1.55
P04792	HSPB1	24	2.88	1.53
P68366	TUBA4A	50	1.73	1.39
Q7L014	DDX46	117	1.43	1.02
P05787	KRT8	54	3.03	1.00

Supplementary Table 5. Cross-linking mass spectrometry results for the BICD2-ScaC complex. Cross-linked residues for BICD2 and ScaC and their respective match scores are indicated. Cross-links within the CC3 domain of BICD2 (residues 711-800) are highlighted.

BICD2 PEPTIDE POSITION	SCAC PEPTIDE POSITION	MATCH SCORE
E800	**K136**	**151**
K814	**K136**	**123**
K771	**E119**	**108**
K785	**K136**	**104**
E138	K39	86
E241	K84	86
K318	E160	79
E216	K39	78
K117	E175	78
K351	K136	68
K771	**E119**	**67**
D316	K136	64
K771	**D122**	**59**
E216	K39	57
D180	K210	57
E216	K39	56
D228	K39	54